Rock Mech Rock Eng (2013) 46:657–681
DOI 10.1007/s00603-012-0294-2

ORIGINAL PAPER

An Investigation of Discontinuity Roughness Scale Dependency Using High-Resolution Surface Measurements

Bryan S. A. Tatone · Giovanni Grasselli

Received: 22 July 2011 / Accepted: 19 July 2012 / Published online: 21 August 2012

Abstract The influence of roughness on the hydro-mechanical behavior of rock discontinuities has long been recognized. As a result, several definitions and measures of roughness have been developed. According to the ISRM (Int J Rock Mech Min Sci Geomech Abstr 15(6):319–368, 1978), discontinuity roughness comprises large-scale (waviness) and small-scale (unevenness) components. However, the division between these scales is not clear and most investigations of surface roughness have been restricted to small fracture surfaces (<1 m^2). Hence, the large-scale components of roughness are often neglected. Furthermore, these investigations typically define roughness using two-dimensional profiles rather than three-dimensional surfaces, which can lead to biased estimates of roughness. These limitations have led to some contradictory findings regarding roughness scale dependency (scale effects). This paper aims to provide some explanation of these contradictory findings. Through the in situ digitization and analysis of two adjacent large-scale ($\sim 2 \times 3$ m^2 and $\sim 2 \times 2$ m^2) migmatitic-gneiss fracture surfaces, the influence of sample size on roughness estimates are investigated. In addition, the influence of measurement resolution on roughness estimates is investigated by digitizing small-scale (100×100 mm^2) samples from the same fracture with varying resolution. The findings show roughness to increase as a function of the sampling window size, in contrast to what is commonly assumed. That is, the combined waviness and unevenness of a discontinuity relative to its mean plane increases with scale. Compared to the sampling window size, the resolution of surface measurements is shown to have a far greater influence on roughness estimates. This influence of measurement resolution may explain some of the contradictory roughness scale relationships that have been published previously. It is important to note that the observed decrease in shear strength with increasing scale, as observed in many prior studies, is not being questioned; rather, a clarification of the role of roughness in this phenomenon is sought.

Keywords Roughness characterization · Roughness scale effect · Roughness anisotropy · Discontinuity roughness · Rock joint roughness

1 Introduction

It has long been recognized that the roughness of rock discontinuities, when clean and unfilled, can have a significant impact on the hydraulic and mechanical characteristics of discontinuous rock masses. In response, several approaches to parameterize roughness have been proposed, including empirical (e.g., Barton 1973; Barton and Choubey 1977), statistical (e.g., Myers 1962; Maerz and Franklin 1990), and fractal methods (e.g., Turk et al. 1987; Lanaro 2000; Kulatilake et al. 2006).

It is also widely recognized that the mechanical behavior of rough rock joints can vary as a function of scale, although the extent is arguable. This scale-dependent behavior is partly attributed to the variation of intact asperity strength and partly to the variation in surface geometry (roughness) with scale (Barton and Choubey 1977). Although it is generally agreed upon that discontinuity roughness comprises a large-scale waviness component and a small-scale

B. S. A. Tatone · G. Grasselli (✉)
Geomechanics Research Group, Department of Civil Engineering, University of Toronto, 35 St. George St, Toronto, ON M5S 1A4, Canada
e-mail: giovanni.grasselli@utoronto.ca

B. S. A. Tatone
e-mail: bryan.tatone@utoronto.ca

unevenness component (ISRM 1978), investigations of surface roughness and scale effects have tended to focus on joint samples <1 m^2. Hence, larger-scale roughness components are rarely measured and accounted for when considering the mechanical behavior of field-scale discontinuities (Fardin et al. 2001).

In addition to inadequately sized fracture surfaces, many roughness investigations have suffered from the conventional approach of characterizing three-dimensional (3D) surface geometry via two-dimensional (2D) linear profiles. This approach, although capable of characterizing pseudo-3D geometry when several profiles in various directions are considered, can lead to incomplete and biased representations of the surface (as noted by McWilliams et al. 1990; Riss and Gentier 1990; Rasouli and Harrison 2004, among others).

For many years, these limitations were difficult to overcome, as tools with sufficient accuracy, resolution, and ease of use were not available to measure 3D surface topography both in situ and in the laboratory. In the 1990s, laboratory laser profilometers began to be employed to obtain high-accuracy surface measurements of discontinuity surfaces (e.g., Huang et al. 1992; Brown 1995). By obtaining a large number of closely spaced profiles, the 3D topography of surfaces could be measured. Nevertheless, with such systems: data acquisition was slow, handling large amounts of data was problematic, and use in situ was not possible.

More recently, several optical instruments have emerged as an attractive alternative to quickly measure discontinuity surfaces in both laboratory and in situ environments. These systems include: laser ranging devices (e.g., Chae et al. 2004; Fardin et al. 2004); close-range terrestrial photogrammetric systems (e.g., Lee and Ahn 2004; Haneberg 2007; Baker et al. 2008); and methods based on structured light projection, such as stereo-topometric cameras (e.g., Grasselli et al. 2002; Hong et al. 2006; Nasseri et al. 2009) and slit scanners (e.g., Belem et al. 1997; Lanaro 2000).

Despite this new found ability to rapidly obtain highly accurate, high-resolution 3D point clouds of both small-scale surfaces in the laboratory and large-scale surfaces in situ, few studies have investigated the roughness of large-scale fracture surfaces and roughness scale effects (Feng et al. 2003; Fardin et al. 2004; Haneberg 2007). Moreover, these few studies have not considered the influence of measurement resolution and noise on roughness estimates although its influence was first identified by Fecker and Rengers (1971) and has since been noted by many others (Yu and Vayssade 1991; Huang et al. 1992; Kulatilake et al. 1995; Seidel and Haberfield 1995; Tatone and Grasselli 2009, among others). As a consequence, the understanding of roughness scale dependency for surfaces beyond 1 m^2 remains limited.

The objective of the current study is therefore twofold. Firstly, it aims to investigate the dependency of roughness on sample size by digitizing two adjacent large-scale natural fracture surfaces ($\sim$6 and $\sim$4 m^2) in situ and evaluating the roughness of sample windows of varying size. Secondly, it investigates the effect of measurement resolution on roughness by digitizing a series of small-scale fracture specimens at different resolutions in the laboratory and evaluating their roughness. In doing so, a further understanding of discontinuity roughness scale effects and, indirectly, shear strength scale effects can be gained.

2 Scale Dependency of Roughness and Shear Strength: a Review

2.1 Conventional View

The widely recognized view on the scale dependency of discontinuity shear strength comes from the work reported by Bandis et al. (1981). By shearing rough discontinuity replicas in the laboratory, they showed that the peak shear strength decreased (negative scale effect) and peak shear displacement (i.e., the amount of displacement required to reach the peak strength) increased as the size of the specimen was increased (Fig. 1). This scale-dependent behavior was attributed partly to the variation of intact asperity strength and partly to the variation in surface geometry (roughness) with scale.

Following an extensive review of existing shear test results along with further shear testing of rock joints and replicas, Barton and Bandis (1982) introduced empirically derived scale corrections for the JRC and JCS terms of the Barton–Bandis shear criterion as

$$\mathrm{JRC_n} = \mathrm{JRC_0}\left(\frac{L_n}{L_0}\right)^{-0.02\mathrm{JRC_0}} \quad (1)$$

$$\mathrm{JCS_n} = \mathrm{JCS_0}\left(\frac{L_n}{L_0}\right)^{-0.03\mathrm{JRC_0}} \quad (2)$$

where $\mathrm{JRC_n}$, $\mathrm{JCS_n}$, and L_n (joint length) represent the values for the joint size of interest; and $\mathrm{JCR_0}$, $\mathrm{JCS_0}$, and L_0 represent the values for a standard 10 cm sample.

It was noted by the developers that the values of JRC and JCS predicted by these equations produce unreasonably low shear strengths when applied to discontinuities over 5 m in length. Thus, it was recommended that the largest value of L_n be limited to the side length of the average block comprising the rock mass. Typically, this block size would be much less than 5 m (Bandis et al. 1981; Barton and Bandis 1990).

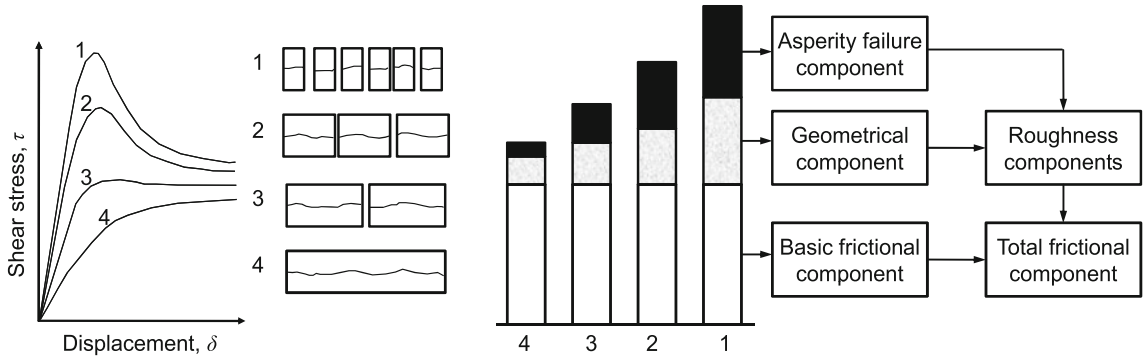

Fig. 1 Conventional view on discontinuity shear strength scale dependence of a rough discontinuity, whereby the asperity strength and surface geometry vary as a function of the sample size (after Bandis et al. 1981)

2.2 Overview of Previous Studies

The scale dependency of discontinuity surface roughness and shear strength has been investigated by many other researchers over the last three decades. Many of these studies have produced conflicting results. Some studies have shown a decrease in strength and roughness with increasing discontinuity size similar to that noted by Bandis et al. (1981) (negative scale effect). Other studies have shown the existence of positive scale effects, a combination of positive and negative scale effects, or no scale effects. Several previous studies of discontinuity roughness scale dependency and shear strength scale dependency are summarized in Tables 1 and 2. For each reference, a brief summary of the main findings with regard to scale dependency of shear strength or roughness is provided. The maximum discontinuity size considered and the type of scale effect observed are also noted (i.e., positive or negative). As a result of these conflicting results, the nature of the scale dependency of both roughness and discontinuity shear strength remain subjects of ongoing debate.

3 Data Acquisition

3.1 Equipment

In this study, the Advanced Topometric Sensor (ATOS II) manufactured by GOM mbH,[1] was used to digitize a large-scale (2×6 m^2) fracture surface in situ and three small-scale (75×75 mm^2 and 100×100 mm^2) samples in the laboratory. The ATOS II and its predecessors were initially developed for quality control and reverse engineering in the automotive industry (GOM 2008). However, the system has now been used for a wide range of 3D measuring applications, including characterizing the geometry of small-scale rock fracture specimens (e.g., Grasselli 2006; Hong et al. 2006; Nasseri et al. 2009; Tatone and Grasselli 2012b).

The ATOS II system consists of a measurement head containing a central projector unit and two CCD cameras, and a high-performance Linux-based PC to pilot the system. The system is flexible in that it can be used in the laboratory with a boom stand and industrial PC or in the field with a laptop and tripod. Figure 2a, b illustrates the laboratory and field setup of the ATOS II, respectively. Due to the lack of availability of a suitable laptop at the time field work was performed for the current study, the industrial PC was transported to the field and powered via a portable generator. Although the ATOS systems have previously been used to investigate rock fracture roughness, this study marks the first use of the system to digitize a rock fracture surface in situ.

The ATOS II measures 3D coordinates via the projection of various structured white-light fringe patterns onto the surface (e.g., Fig. 2b, c). Images of these patterns, which become distorted due to the relief of the surface, are captured automatically by the two CCD cameras. With the relative offset and angle between the projector and cameras known, the software computes precise 3D coordinates for each pixel in these images using the principle of triangulation. With the $1{,}392 \times 1{,}040$ pixel CCD cameras used in the current study, up to roughly 1.4 million measurement points could be obtained in a single measurement (GOM 2008). Depending on the selected camera shutter speeds, one measurement requires 1–10 s to be completed.

While the number of measurement points that can be acquired in a single measurement is dictated by the size of CCD chips, the average spacing (resolution) of theses points can be varied by changing the measuring distance, that is, the distance between the sensor and the object being scanned. For a given measuring distance, different camera and projector lenses are required to obtain focused images.

[1] http://www.gom.com/metrology-systems/system-overview/atos.html.

Table 1 Summary of previous studies that examined the scale dependence of discontinuity roughness through the measurement and analysis of surface topography

References	Description of study	Discontinuity size (area or length)	Surface measurement methodology	Observed scale effects
Swan and Zongqi (1985)	As part of a study on the prediction of rock joint shear behavior, the roughness of 2D profiles from two different discontinuities was evaluated. Roughness (root mean square of the profile height) was shown to both increase and decrease with increasing profile length depending on the selected reference line	0.9–54 cm	Stylus profilometer (point spacing $\sim$0.6 mm)	*Positive scale effect* when unique reference lines for each profile length were used. *Negative scale effect* when a single common reference line was used for all profile lengths
Maerz and Franklin (1990)	To study roughness scale effects, these authors measured two large profiles from two different discontinuity exposures via shadow profilometry. Subsequently, the roughness of the profiles was assessed using several textural and amplitude roughness parameters	10–500 cm	Shadow profilometry (point spacing = 0.4–10 mm)	*Negative scale effect* for textural roughness parameters. *Positive scale effect* for amplitude roughness parameters
Cravero et al. (1995)	As part of this study, common statistical parameters and the fractal dimension were used to characterize varying length-roughness profiles with both constant (1 cm) and varied point spacing (1 % of profile length)	20–1,000 cm	Mechanical profilometer used to acquire 20-cm profiles (point spacing = 1 cm) coupled with manual height measurements (point spacing = 20 cm) permitted reconstruction of 10-m profile with 1-cm spacing	*Positive scale effect* with constant point spacing. *Negative scale effect* with scaled point spacing
Cravero et al. (2001)	In this study, the topography of natural schist discontinuities was measured in the field via photogrammetry and in the laboratory with a profilometer. From 2D profiles of varying length, values of Z_2, dilation angle (i), and fractal dimension (D) were computed to examine the influence of sample length	6–500 cm	Digitization via photogrammetry and profilometer (point spacing = 50 and 3 mm and 0.7 and 0.1 mm, respectively)	*Negative scale effect* with all roughness indices decreasing with increasing profile length
Leal-Gomes (2003)[a]	In this study, the shear strength and surface topography of variously sized joint replicas were investigated. The replicas were cast from one artificial tensile fracture in granite. The average amplitude of surface asperities was found to increase with replica size and pull tests showed the shear strength to increase as well	84–256 cm^2	Details not provided	*Positive scale effect* with the average amplitude of surface asperities increasing with specimen size
Fardin et al. (2001)	In this study, the scale dependence of roughness was investigated by digitizing a 1-m^2 silicon replica of a natural rock discontinuity in the laboratory and analyzing the roughness of increasingly larger sampling windows. Digitization was performed with a slit scanner and the 3D roughness was evaluated using the fractal dimension (D) and a related amplitude parameter (A)	100 – 1 $\times$ 10^4 cm^2	Automated slit scanner (point spacing = 0.2 mm)	*Negative scale effect* for fractal dimension and amplitude parameter

Table 1 continued

References	Description of study	Discontinuity size (area or length)	Surface measurement methodology	Observed scale effects
Fardin et al. (2004)[b]	As a follow-up to Fardin et al. (2001), this study considered the roughness of a 4-m^2 fracture that was digitized in situ with a LIDAR system. Again, to investigate roughness scale dependence, the roughness of increasingly larger sampling windows was evaluated using 3D fractal parameters	1×10^4–4×10^4 cm^2	LIDAR (point spacing = 5 mm)	*Negative scale effect* for fractal dimension and amplitude parameter
Fardin (2008)	As part of this study, the roughness of increasingly larger areas of 4 fracture surfaces was investigated using the same approach as described in Fardin et al. 2001. However, the fractal parameters, *D* and *A*, decreased as the sampling window was enlarged	25–400 cm^2	Automated slit scanner (point spacing = 0.2 mm)	*Positive scale effect* for fractal dimension and amplitude parameter

[a] Details of asperity amplitude measurement not provided

[b] Roughness was evaluated after decimating point spacing to 20 mm due to problems with measurement noise

The camera offset and inter-camera angle must also be varied to permit triangulation. The current study utilized four different sensor configurations. The nominal point spacing, measuring volume, and measuring distance for these configurations are summarized in Table 3.

The ATOS system can only calculate 3D coordinates for the pixels visible in both the left and the right images. Therefore, complete digitization of a surface typically requires several individual measurements from different positions. Reference points (adhesive circular markers), which are applied directly to the surface to be digitized as in Fig. 2b, c, are used to properly and automatically position each of these measurements into a common global coordinate system. Based on the first measurement of the surface, the system establishes an arbitrary global coordinate system and identifies any reference points in the field of view. For all subsequent measurements, the system automatically identifies new and previously defined reference points and uses the previously defined points to automatically transform the current measurement into the global coordinate system. At least three previously defined reference points must be visible to complete this transformation (GOM 2008).

After obtaining measurements over the area of interest, the data from each individual measurement are used to polygonize the surface. This process involves alignment of the individual measurements to minimize the deviations between overlapping areas and, subsequently, deleting redundant data. A continuous triangulated irregular network (TIN) mesh of the surface is then obtained. This mesh can be exported from the ATOS system in a variety of 3D file formats or as an ASCII point cloud (vertices of the triangular facets). For the current study, the digitized fracture surfaces were reconstructed using the default triangulation algorithm (Delaunay triangulation without smoothing) and exported in binary stereolithography (*.STL*) format, a ubiquitous 3D file format in the rapid prototyping industry.

3.2 Description of Digitized Discontinuity Surface

To study the dependency of fracture roughness on sampling window size, a large, exposed fracture surface that could be easily digitized was sought. A suitable fracture surface was found in a relatively new road-cut (~5 years old) nearly 200 km north of Toronto, Ontario, Canada along the northbound off-ramp of Exit 189 of Provincial Highway 400 (45°05′37″N, 79°46′54″W). The rock-cut extends nearly 200 m through a medium-grained migmatitic-gneiss rock mass and reaches a maximum height of approximately 7 m. The cut face is oriented sub-parallel to a persistent subvertical fracture set that strikes roughly NNE–SSW. As a result, the face contains several large exposures of natural, planar to undulating fracture surfaces showing slight alteration (Fig. 3a). At the scale of the exposed fracture surface, the migmatitic foliation is incoherent with no obvious preferred orientation.

To study the impact of measurement resolution on roughness estimates, three small-scale samples (Fig. 4a) were collected from the field site. These samples were transported to the University of Toronto where they were digitized at varying resolution with the ATOS II system in the laboratory.

Table 2 Summary of previous studies that examined the scale dependence of discontinuity shear strength through shear testing

References	Description of study	Discontinuity size (area or length)	Shear testing and/or surface measurement methodology	Observed scale effects
Pratt et al. (1974)	Regarded as the first comprehensive study of discontinuity scale effect; a combination of in situ and laboratory shear tests on quartz diorite samples of varying size was performed to investigate the effect of size on shear strength and stiffness	60–5,000 cm^2	Combination of laboratory direct shear tests and in situ shear tests using a system of flat jacks	*Negative scale effect* where shear strength decreased with increased sample size
Kutter and Otto (1990)	As part of this study, a combination of artificial gneiss fractures and natural joint replicas of varying size was shear tested with a base friction machine. The influence of sample size was quantified using the mean peak dilation angle observed during shearing	77–1,220 cm^2	Direct shear testing (normal loading conditions not specified)	*Positive scale effect* for specimens with well-matched surfaces. N*egative scale effect* for specimens with poorly matched surfaces
Muralha and Pinto Da Cunha (1990)	This paper summarizes the scale effects of discontinuity shear strength based on the results of several shear testing programs. The test results were acquired via a combination of laboratory and in situ tests. Although the results displayed significant scatter, average shear strengths decreased with increasing sample size	28–5,000 cm^2	Combination of direct shear tests in the laboratory and in situ shear tests ($\sigma_n = 0.1 - 1.5$ MPa)	*Negative scale effect* where shear strength decreased with increased sample size
Giani et al. (1995)	As part of this study, tilt tests were performed on discontinuity specimens of gneiss and syenite of varying size to establish a relationship between discontinuity size and back-calculated JRC values	50–1,560 cm^2	Tilt testing to back-calculate JRC according to Barton (1973)	*Positive scale effect* for gneiss specimens. *Negative scale effect* for the syenite specimens
Hencher et al. 1993)	This study aimed to confirm the findings of Bandis et al. (1981) by testing similar specimens and following, as closely as possible, the same experimental methodology	44–531 cm^2	Direct shear testing ($\sigma_n = 24.5$ kPa)	*No scale effect* as samples of various sizes showed large, non-systematic variation in peak strength
Ohnishi and Yoshinaka (1995)	This study examined the shear strength of replicas of a natural joint surface of various size and saw-toothed surfaces of various size. The effect of the sample size was quantified via CNS direct shear tests	100–1,000 cm^2	Direct shear testing (CNS conditions with $\sigma_n = 0.26 - 2.04$ MPa)	*Negative scale effect* for natural joint replicas. *No scale effect* for joints comprising regular triangular asperities
Castelli et al. (2001)	In this study, a series of 10- and 20-cm square replicas cast from a larger artificial tension joint were shear tested in the laboratory. Subsequently, the influence of the sample size on the peak displacement, peak friction angle, joint stiffness, dilation angle and estimated contact area was compared	100–200 cm^2	Direct shear testing ($\sigma_n = 0.75$, 1.5, and 3.0 MPa)	*Negative scale effect* for all roughness indices considered, yet only 2 specimen sizes were considered
Leal-Gomes (2003)	In this study, the shear strength and surface topography of variously sized joint replicas were investigated. The replicas were cast from one artificial tensile fracture in granite. The average amplitude of surface asperities was found to increase with replica size and pull tests showed the shear strength to increase as well	84–256 cm^2	Pull testing (CNL, $\sigma_n = 1$ kPa)	*Positive scale effect* with back-calculated *JRC* values appearing to approach a constant value for the larger specimens tested

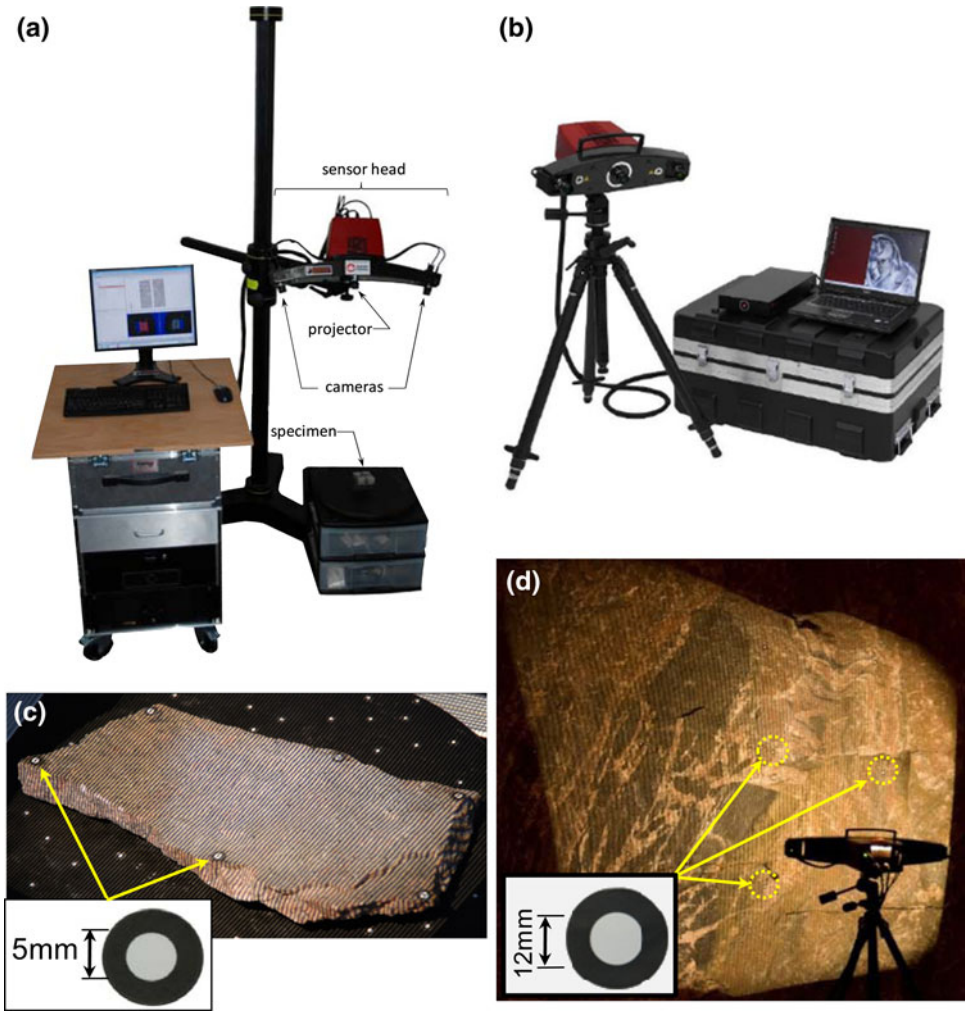

Fig. 2 **a** Laboratory configuration and **b** field configuration of the Advanced Topometric Sensor (ATOS) II manufactured by GOM mbH that was utilized in this study to digitize discontinuity surfaces, **c** distorted fringes as projected on a laboratory-scale and **d** field-scale fracture surface

3.3 In situ Digitization Procedure

In the field, a total area, roughly 6-m wide by 2-m high, was digitized using the first ATOS configuration listed in Table 3. As shown in Fig. 3, the digitized area consisted of two large fracture surfaces separated by a 0.3-m deep step. These two surfaces were digitized individually and subsequently merged together into one large 3D model (Fig. 3b). Starting from the center of each surface and working outward in a radial pattern, as shown in Fig. 3a, nine individual measurements were needed to digitize each surface. A 0.6-m × 0.6-m grid of 12-mm diameter reference points affixed to the fracture surface with a small amount of epoxy facilitated transformation of each measurement into a common global coordinate system (Fig. 2d). The 3D TIN model of the entire digitized area (Fig. 3b) contained approximately 8.2 million points and 16.3 million triangles. The computed mesh deviation of this model was 0.181 mm. This value quantifies the average deviation between redundant data (i.e., overlapping measurements). Hence, it serves as an estimate of the intensity of the average measurement noise in the 3D data (GOM 2008). At the time of writing, these data are of the highest resolution ever obtained while digitizing a fracture surface greater than 1 m^2.

Table 3 Summary of the measuring volume, point spacing, and measuring distance of the four ATOS II configurations employed in the current study

ATOS configuration	Measuring volume [l × w × h] (mm^3)	Nominal point spacing (mm)	Measuring distance (mm)
1	1,400 × 1,120 × 952	1.0	1,400
2	700 × 560 × 476	0.5	1,030
3	350 × 280 × 238	0.25	1,030
4	55 × 44 × 37.5	0.04	280

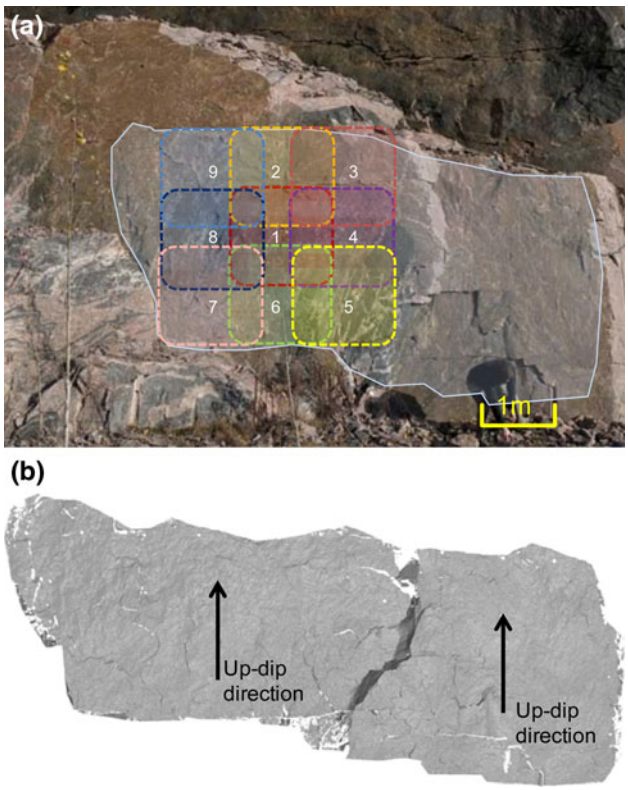

Fig. 3 **a** Photograph showing the large-scale fracture surface selected for digitization and the measurement sequence; **b** complete 3D model of the fracture surface (8.2 million measurement points with a nominal spacing of 1.0 mm)

Since the ATOS system uses fringe projection to calculate 3D coordinates, the projected patterns had to be clearly visible to the CCD cameras. Since bright ambient light can be problematic in this regard, the measurement of the fracture was performed in the evening. It should be noted that more recent ATOS systems have overcome the problems related to strong ambient lighting.[2]

The total time required for two people to perform the data acquisition in the field was nearly 1.5 h. An additional 45 min was required to combine the two measurement projects (for the left and right surfaces) and generate the final surface mesh. Given that this field work represented the authors' first experience using the ATOS II in the field, it is anticipated that a similarly sized fracture could be digitized in less than 1 h in the future.

3.4 Laboratory Digitization Procedure

In the laboratory, with the ATOS II mounted on a boom stand (Fig. 2a), the fracture samples collected in the field were digitized with each configuration listed in Table 3. Considering the measuring volume of the first three

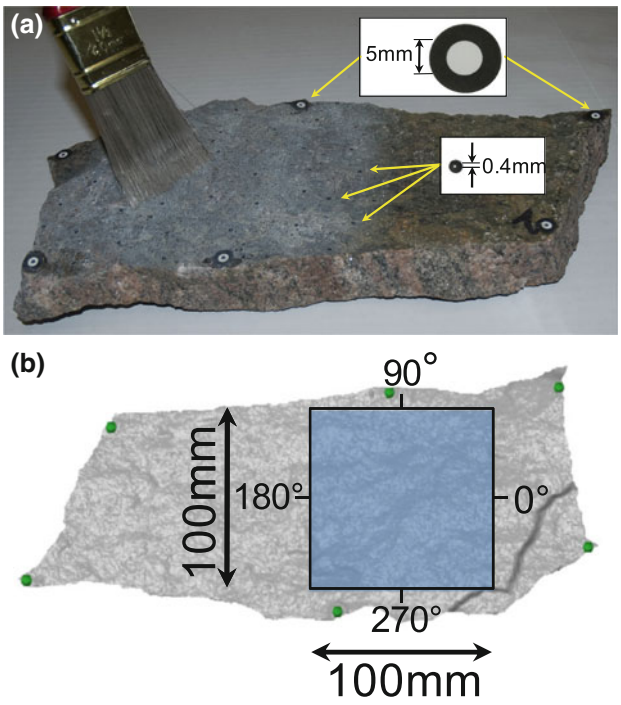

Fig. 4 **a** Photograph of one of the small-scale fracture samples (Sample 2) showing the 5- and 0.4-mm reference points used to transform each measurement into a common coordinate system and the talc powder brushed on to surfaces to dull minerals with vitreous luster; **b** example of the digitized surface overlain with the square sampling windows used for roughness analysis (*note* the orientation marked 0°, 90°, 180°, and 270° correspond to the angles on the polar plots of roughness presented in Sect. 6)

configurations relative to the size of the samples, complete digitization required only one to two measurements. Thus, only four to seven 5-mm reference points were needed around the perimeter of each sample to permit transformation of each individual measurement into a common coordinate system (Fig. 4a). The fourth configuration (0.044-mm point spacing) had a significantly smaller measuring volume; hence, digitization of each sample required several measurements. Therefore, similar to the field procedure, the surface of each sample was digitized using a radial measurement pattern where several 0.4-mm diameter reference points enabled transformation of individual measurements into a common global coordinate system (Fig. 4a). Digitization with the fourth configuration also required the fracture samples to be lightly dusted with talc powder, as shown in Fig. 4a. The talc powder acted to dull the vitreous luster of mineral grains that would otherwise result in overexposure of some pixels when photographed by the CCD cameras.

Following digitization with each ATOS configuration, the resulting 3D models were transformed into a common coordinate system via common reference points. Afterward, square sampling windows, as outlined in Fig. 4, were exported for roughness analyses. The total number of

[2] http://www.gom.com/metrology-systems/system-overview/atos.html.

Table 4 Summary of the total number of measurement points and corresponding mesh deviations obtained with each ATOS configuration when digitizing the sampling windows illustrated in Fig. 4b

ATOS configuration	Nominal point spacing (mm)	Total number of points			Mesh deviation (mm)
		Sample 1	Sample 2	Sample 3	
1	1.000	5,589	10,079	10,270	~0.050
2	0.500	19,289	34,551	34,823	~0.020–0.025
3	0.250	154,565	279,586	279,711	~0.010–0.013
4	0.044	2,622,181	4,809,868	4,897,906	~0.004–0.006

Table 5 Summary of roughness parameters employed to study the scale dependency of discontinuity roughness

Parameter	2D or 3D	Description	References
Directional roughness parameters			
$\theta^*_{max}/[C+1]$	3D	$\theta^*_{max}/[C+1]$ characterizes the distribution of the apparent dip (in any direction) of each triangular facet of a TIN surface. The greater the proportion of steeply dipping triangles, the rougher is the surface and the larger the value of $\theta^*_{max}/[C+1]$	Tatone and Grasselli (2009)
$\theta^*_{max}/[C+1]_{2D}$	2D	$\theta^*_{max}/[C+1]_{2D}$ is the 2D variant of $\theta^*_{max}/[C+1]$. It characterizes the distribution of the inclination (in the forward or reverse direction) of each line segment of a 2D roughness profile. The greater the proportion of steeply dipping line segments, the rougher is the surface and the larger the value of $\theta^*_{max}/[C+1]_{2D}$	Tatone and Grasselli (2010)
Non-directional roughness parameters			
D and A[a]	3D	D and A are the fractal dimension and amplitude parameter, respectively, as determined from 3D roughness-length analysis procedure. These parameters describe the self-affine fractal geometry of the surface. Higher values of D and A are indicative of a rougher surface	Lanaro (2000); Fardin et al. (2001)
R_S	3D	R_s is defined as the ratio of the true fracture surface area to its nominal surface area. Rougher surfaces display greater ratios as the true surface area is larger due to its increased undulation and unevenness	El-Soudani (1978)
Z_2	2D	Z_2 is defined as the root mean square of the first derivative of the profile height. Larger values of Z_2 are indicative of a rougher surface	Myers (1962)
R_P	2D	R_P is the 2D equivalent of R_s. It is defined as the ratio of the true length of a 2D roughness profiles to its nominal length. Rougher profiles display greater ratios as the true profile length is larger due to its increased undulation and unevenness	El-Soudani (1978)

[a] The 3D roughness-length method represents an adaptation of the 2D methodology developed by Malinverno (1990) with consideration of the recommendations for 2D analysis proposed by Kulatilake and Um (1999)

measurement points and range of computed mesh deviations for each of these sampling windows is summarized in Table 4. Using these configurations, the total number of points characterizing the sampling windows varied by three orders of magnitude, while the average mesh deviation only varied by one order of magnitude.

4 Roughness Parameterization

The TIN surface models obtained with the ATOS II system merely provide a qualitative description of the surface roughness. An objective parameterization of the roughness requires further processing and analysis of the 3D measurements. Several methods to parameterize the roughness of rock discontinuities have been proposed, including 2D parameters based on 2D surface profiles and 3D parameters that consider the entire discontinuity surface. In the current study, a variety of 2D and 3D roughness parameters have been considered. Thus, any differences in the scaling behavior related to the selected roughness parameters could be identified. The goal was not to show any one parameter as superior, but rather determine if general trends in roughness with scale and resolution were consistent amongst different roughness metrics.

The roughness parameters considered in the current study can be divided into two categories: directional and non-directional. Directional parameters are those that capture differences in roughness in different directions along the surface. That is, given a 2D profile or 3D surface, differences in the roughness in the forward and reverse direction can be characterized. Non-directional parameters define roughness independent of direction. That is, they may be able to characterize roughness anisotropy by

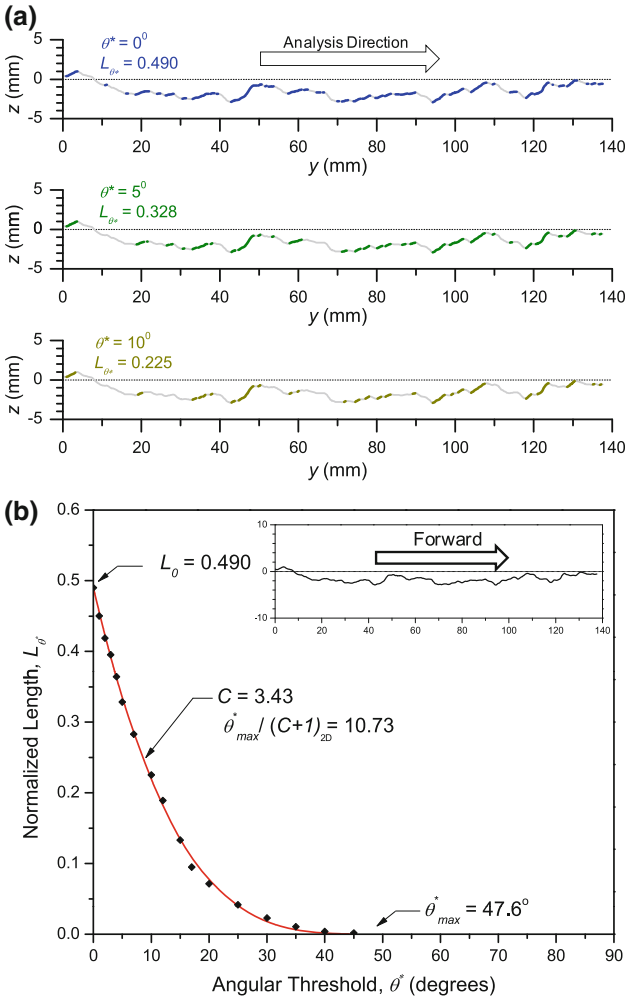

Fig. 5 **a** Example of a 2D profile showing normalized fractional length (L_{θ^*})corresponding to angular thresholds (θ^*) of 0°, 5°, and 10°; **b** plot of L_{θ^*} versus θ^* with a best-fit curve given by Eq. (3) (after Tatone and Grasselli 2010)

considering profiles oriented in different directions, but they are unable to resolve differences in roughness in the forward and reverse direction along a single profile. Table 5 summarizes the roughness parameters used to evaluate roughness scale effects in the current study.

4.1 Directional Roughness: $\theta^*_{max}/[C+1]$ and $\theta^*_{max}/[C+1]_{2D}$

The parameters $\theta^*_{max}/[C+1]$ and $\theta^*_{max}/[C+1]_{2D}$ characterize the cumulative distribution of the apparent inclination of the triangular facets of a TIN surface and the inclination of the line segments of a 2D profile, respectively.

Considering a 2D profile composed of straight line segments or a 3D surface composed of 3D triangular facets, it is possible to determine the fraction of the profile length or surface area inclined more steeply than particular angular threshold values, θ^*. This fractional length or area is normalized with respect to the total profile length or surface area, respectively. Figure 5 illustrates this concept for a 2D profile. Considering threshold values of θ^* equal to 0°, 5°, and 10°, the corresponding normalized lengths (L_{θ^*}) are 0.490, 0.328, and 0.225. If additional values of θ^* up to a maximum of 90° are considered, a power law relationship of the following form can be established between the normalized length (L_{θ^*}) or area (A_{θ^*}) and θ^*, as (Tatone and Grasselli 2009, 2010):

$$L_{\theta^*} = L_0\left(\frac{\theta^*_{max}-\theta^*}{\theta^*_{max}}\right)^C \quad \text{or} \quad A_{\theta^*} = A_0\left(\frac{\theta^*_{max}-\theta^*}{\theta^*_{max}}\right)^C \tag{3}$$

where L_0 and A_0 are the normalized length and normalized area corresponding to $\theta^* = 0°$, respectively; θ^*_{max} is the inclination of steepest segment or facet; and C is a fitting parameter that describes the shape of the cumulative distribution.

A higher proportion of steeply inclined segments or facets is indicative of a rougher surface and is reflected by a larger area under the curve given by (3). Although the area under the curve is equal to $2(L_0 \text{ or } A_0)\theta^*_{max}/[C+1]$, L_0 and A_0 are typically very close to 0.5. Thus, the roughness metric is taken as $\theta^*_{max}/[C+1]$. The subscript '2D' is added to differentiate between values based on 2D profiles from those based on 3D surfaces. Further details regarding this roughness evaluation methodology are provided in Tatone and Grasselli (2009, 2010).

4.2 3D Roughness-Length Method

Since the popularization of fractal geometry by Mandelbrot (1967, 1983), several researchers have attempted to use it to characterize rock discontinuity roughness. Although much of the effort in this direction has been focused on the characterization of 2D profiles, some 3D methods have been developed. The 3D roughness-length method (Lanaro 2000; Fardin et al. 2001) is one method to estimate the fractal parameters (fractal dimension, D, and amplitude parameter, A) describing the roughness of a 3D surface. This method is based on the 2D roughness-length method originally developed by Malinverno (1990) and takes into consideration the recommendations for 2D analysis proposed by Kulatilake and Um (1999). To date, the 3D roughness-length method has been used to characterize the roughness of rock discontinuities in several studies (e.g., Feng et al. 2003; Fardin et al. 2004; Rahman et al. 2006; Fardin 2008).

In applying the 3D roughness-length method, the surface to be analyzed is divided into a grid of square local sampling windows with side length w, as shown in Fig. 6.

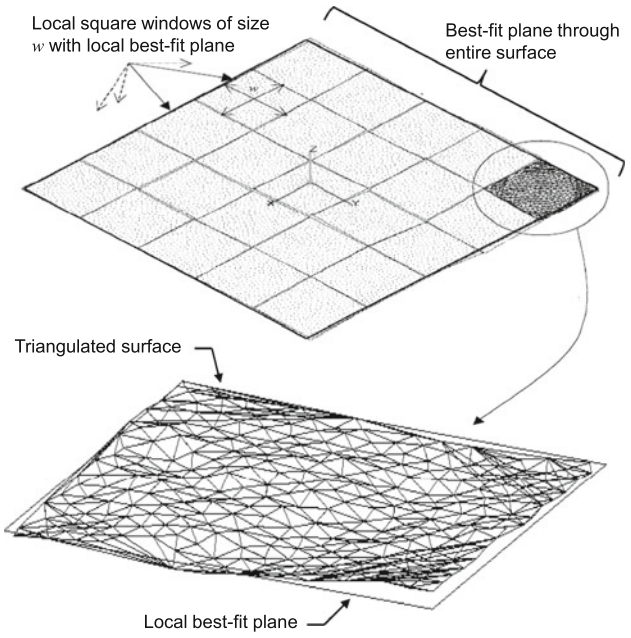

Fig. 6 Schematic showing the measurement of the residual surface heights for the 3D roughness-length method (after Fardin et al. 2001)

Subsequently, local best-fit planes are constructed through each of these windows via least-square regression. The residual surface heights, defined as the perpendicular distance between points that make up the surface and the local best-fit plane, are then measured. There is a power law relationship between the standard deviation of the residual surface heights, $S(w)$, and local window length, w, as follows (Malinverno 1990):

$$S(w) = Aw^H \tag{4}$$

where A is a proportionality constant that describes the surface amplitude and H is the Hurst exponent (Kulatilake and Um 1999; Fardin et al. 2001). The Hurst exponent is related to the fractal dimension, D, as $H = E - D$, where E is the Euclidean dimension (i.e., $E = 2$ for a 2D profile and $E = 3$ for a 3D surface). The value of D is an index for the spatial autocorrelation of the z-coordinates defining the surface (Brown and Scholz 1985; Kulatilake and Um 1999). It can range from a minimum of two for a flat surface to a maximum of three for a very complex, irregular, interconnected surface. Rock discontinuities typically display D values <2.5. For a 3D surface, $S(w)$ is calculated as (Fardin et al. 2001):

$$S(w) = \mathrm{RMS}(w) = \frac{1}{n_w}\sum_{i=1}^{n}\sqrt{\frac{1}{m_i - 2}\sum_{j\in w}(z_j - \bar{z})^2}, \tag{5}$$

where n_w is the total number of local sampling windows of side length w; m_i is the number of points in the ith window; z_j is the residual surface height for the jth measurement point in the ith window; and $\bar{z}$ is the mean residual surface height in the ith window.

4.3 Roughness Coefficients: R_s and R_p

Two commonly employed discontinuity roughness parameters are the 2D and 3D roughness coefficients, R_P and R_S. These parameters provide a measure of the irregularity of 2D profiles and 3D surfaces relative to a best-fit line or plane, respectively.

R_P is defined as the ratio of the true profile length, L_t, to the nominal profile length, L_n (El-Soudani 1978):

$$R_P = \frac{L_t}{L_n} = \frac{\sum_{i=1}^{N-1}\sqrt{(x_{i+1} - x_i)^2 + (y_{i+1} - y_i)^2}}{L_n} \tag{6}$$

where (x_i, y_i) and (x_{i+1}, y_{i+1}) represent adjacent coordinates of a 2D profile and N represents the total number of points defining the profile. The nominal length, L_n, is given by the projection of the 2D profile onto its best-fit line.

R_s is the 3D analog of R_P, defined as the ratio of the true surface area, A_t, to the nominal surface area, A_n (El-Soudani 1978):

$$R_S = \frac{A_t}{A_n} \tag{7}$$

According to these methods, a perfectly flat surface will have a value equal to 1 and rougher surfaces will display values up to 2 for rock discontinuities due to the increased undulation and unevenness of the surface.

4.4 Root Mean Square of Profile Slope: Z_2

The parameter Z_2 represents the root mean square of the first derivative of the height of a 2D profile. For a 2D profile defined by N coordinate pairs over a length L, Z_2 is given by (Myers 1962):

$$Z_2 = \sqrt{\frac{1}{L}\int_{x=0}^{x=L}\left(\frac{\mathrm{d}y}{\mathrm{d}x}\right)^2 \mathrm{d}x} \approx \sqrt{\frac{1}{L}\sum_{i=1}^{N-1}\frac{(y_{i+1} - y_i)^2}{(x_{i+1} - x_i)}} \tag{8}$$

where (x_i, y_i) and (x_{i+1}, y_{i+1}) represent adjacent coordinates separated by a constant Δx.

4.5 Roughness Anisotropy

In the current study, the anisotropy in roughness and its variation with scale is also considered. Roughness anisotropy is illustrated by plotting roughness parameters obtained in different directions on polar plots. For this study, anisotropy is quantified as the ratio of the maximum directional roughness to the minimum directional roughness (2D or 3D) in any direction.

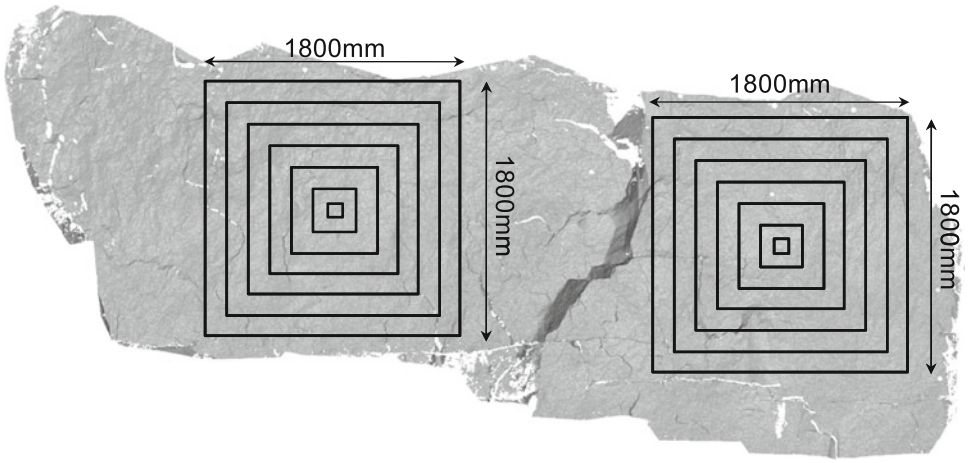

Fig. 7 Size and location of square sampling windows (100 mm × 100 mm to 1,800 mm × 1,800 mm) on the large-scale digitized fracture surfaces

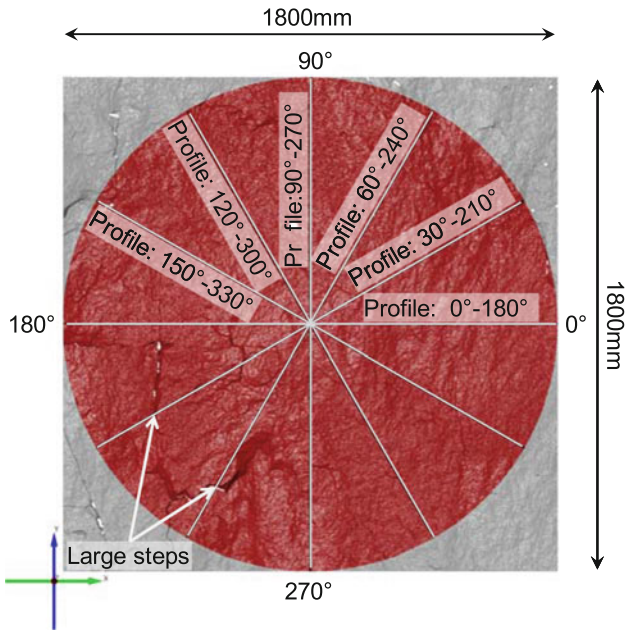

Fig. 8 Example of the location and orientation of the six 2D profiles extracted from a square sampling window

5 Influence of Sampling Window Size

5.1 Methodology

To examine the sensitivity of the 3D roughness parameters to sample size, varying sized sub-areas (sample windows) from the large-scale fracture digitized in situ were analyzed. Seven concentric square and seven concentric rectangular sampling windows located on both the left and right fracture surfaces were considered. Figure 7 illustrates the square sampling windows considered. The rectangular widows were centered at the same locations and measured from 100 × 64 mm^2 to 2,800 × 1,800 mm^2 on the left surface and from 100 × 126 mm^2 to 1,750 × 2,200 mm^2 on the right surface. To serve as a reference for measuring the different roughness parameters, a unique best-fit plane was established through each sampling window. Subsequently, each window was transformed such that the best-fit plane defined the xy-plane ($z = 0$). The y-axis was aligned parallel with the line of maximum dip with the positive y-direction oriented in the up-dip direction defined in Fig. 3b.

To examine the sensitivity of the 2D roughness parameters to sample window size, a series of six 2D profiles were extracted from each square sampling window at angular increments of 30° and analyzed. By cropping the square sampling windows into circles, profiles of the same nominal length were obtained, as shown in Fig. 8.

5.2 Results of Directional Roughness Evaluation

The 3D and 2D directional roughness results, $\theta^*_{\max}/[C+1]$ and $\theta^*_{\max}/[C+1]_{2D}$, for the right square sampling windows of the large-scale fracture are displayed in the polar plots in Fig. 9.[3] The variation in roughness over the range of window sizes was approximately 2–3 roughness units. The figure shows that, in nearly all directions, the 3D roughness increases with expanding window size (i.e., positive scale effect). The presence of a positive scale effect in the 2D values is less apparent. While some orientations (e.g., 0° and 150°) show a distinct positive scale effect, the relationship between 2D roughness and window size in other directions is essentially random.

The inconsistency in the scale effect displayed by the 2D results can be attributed to the use of single profiles for each orientation. Since parallel and offset 2D profiles typically display a range of roughness values with a mean

[3] Since the results for the left and right rectangular and square windows were found to display similar trends, only the results from the right square sampling windows are plotted herein.

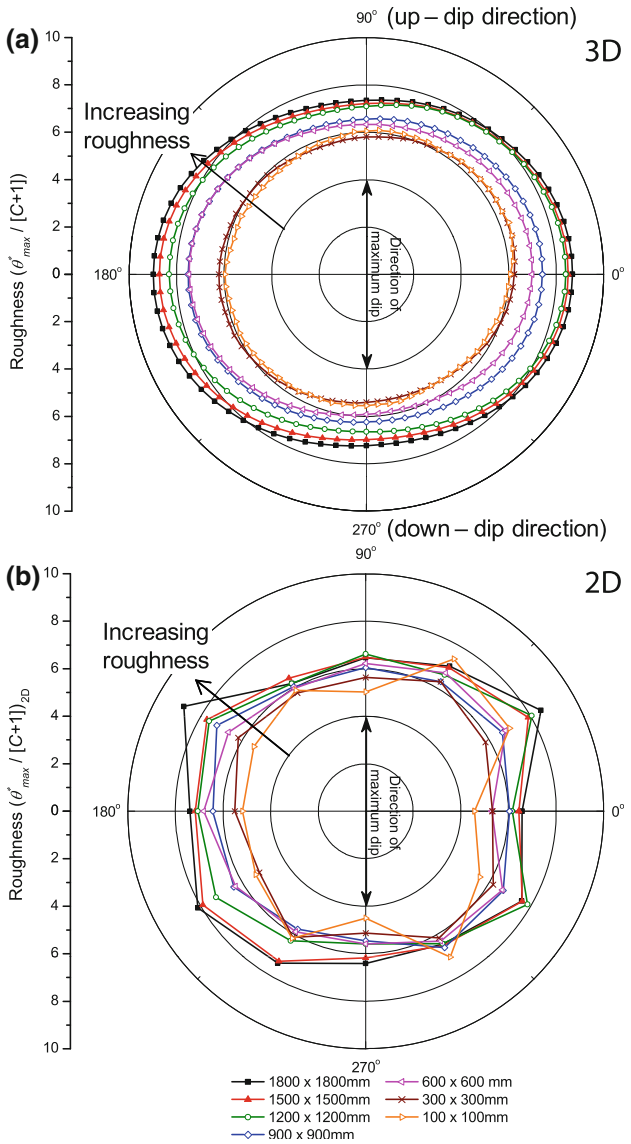

Fig. 9 **a**, **b** Polar plots of the 3D and 2D directional roughness ($\theta^*_{max}/[C+1]$ and $\theta^*_{max}/[C+1]_{2D}$), respectively, for the square sampling windows on the right fracture surface (*note* the 0° and 90° directions are perpendicular and parallel to the up-dip direction defined in Fig. 3b, respectively)

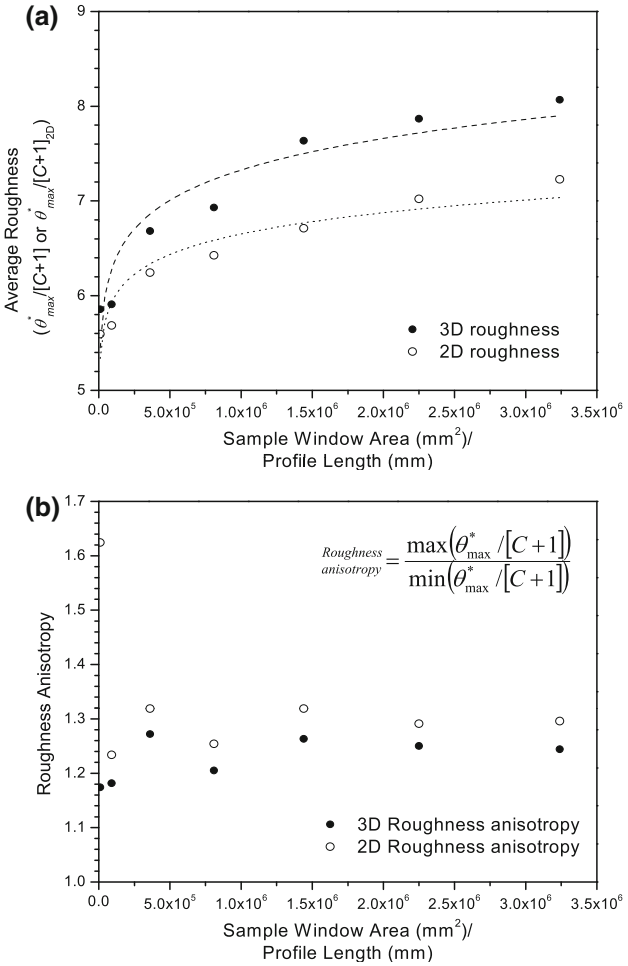

Fig. 10 **a** Average 3D and 2D directional roughness (mean $\theta^*_{max}/[C+1]$ and mean $\theta^*_{max}/[C+1]_{2D}$) and **b** 3D and 2D roughness anisotropy ($\max\{\theta^*_{max}/[C+1]\}/\min\{\theta^*_{max}/[C+1]\}$ and $\max\{\theta^*_{max}/[C+1]_{2D}\}/\min\{\theta^*_{max}/[C+1]_{2D}\}$) as a function of sampling window size for the right fracture surface

value approximating the 3D roughness (Tatone and Grasselli 2010), the results from single profiles may vary from the corresponding 3D values by differing amounts.

Plotting of the average 3D and 2D roughness values as a function of sample window size (Fig. 10) further illustrates the positive scale effect.[4] A 34 % difference is observed between the average 3D roughness values for the smallest and largest windows and a 25 % difference is observed in the 2D roughness values for longest and shortest profiles. The trend shown in the plots suggests that the roughness may approach a constant value for windows larger than 3×10^6 mm^2. The lower values of 2D roughness compared to 3D roughness may also be related to the use of single profiles in each analysis direction. The values of the average 2D and 3D roughness are given in Table 6.

The concentric ellipses formed by the 3D data series in Fig. 9a indicate that the roughness anisotropy is consistent for the sampling windows considered. That is, the ratio of the highest to lowest roughness value was similar for all sampling windows. The lowest and highest roughness values are observed along the line of maximum dip (90°–270°) and perpendicular to the direction of maximum dip (0°–180°), respectively. The 2D roughness values in Fig. 9b show a similarly orientated elliptical shape, but with a more irregular shape.

The values of roughness anisotropy for the right square sampling windows are plotted as a function of sample size

[4] The 'average' values of $\theta^*_{max}/[C+1]$ and $\theta^*_{max}/[C+1]_{2D}$ are represent mean of the values calculated at each orientation.

Table 6 Summary of roughness parameters obtained for the square sampling windows

Sampling window size (mm^2)	Discontinuity roughness						
	Mean $\theta^*_{max}/[C+1]$	Mean $\theta^*_{max}/[C+1]_{2D}$	D	A	R_S	Mean R_P	Mean Z_2
Left square							
100 × 100	7.39	6.76	–	–	1.0031	1.0125	0.159
300 × 300	7.25	7.32	2.252	0.0199	1.0176	1.0141	0.187
600 × 600	7.25	6.98	2.214	0.0179	1.0230	1.0129	0.173
900 × 900	7.51	7.19	2.201	0.0190	1.0292	1.0135	0.177
1,200 × 1200	7.51	7.19	2.229	0.0208	1.0297	1.0138	0.183
1,500 × 1500	7.66	7.26	2.227	0.0214	1.0325	1.0142	0.185
1,800 × 1800	7.92	7.40	2.202	0.0215	1.0390	1.0157	0.202
Right square							
100 × 100	5.86	5.59	–	–	1.0021	1.0094	0.146
300 × 300	5.91	5.69	2.272	0.0182	1.0081	1.0090	0.140
600 × 600	6.68	6.24	2.227	0.0179	1.0196	1.0112	0.162
900 × 900	6.93	6.42	2.244	0.0191	1.0222	1.0118	0.164
1,200 × 1200	7.63	6.71	2.184	0.0185	1.0380	1.0126	0.183
1,500 × 1500	7.87	7.02	2.186	0.0197	1.0410	1.0178	0.221
1,800 × 1800	8.07	7.23	2.183	0.0195	1.0420	1.0179	0.220

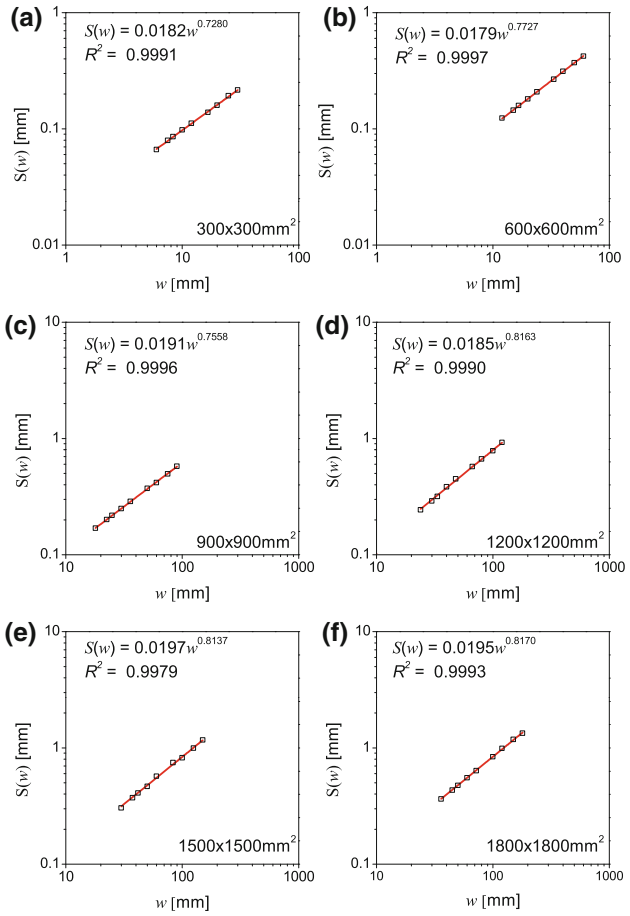

Fig. 11 **a–f** Log–log plots of $S(w)$ versus w for the six square sampling windows on the right fracture surface

in Fig. 10b. Roughness anisotropy is highly variable for the smallest sampling windows and becomes relatively consistent with increasing sample window size. The anisotropy based on the 3D roughness values is less than that obtained from the 2D roughness values. The irregular shape of the polar plot of 2D roughness values based on single profiles in each analysis direction led to the comparatively higher anisotropy values.

5.3 Results of Non-Directional Roughness Evaluation

5.3.1 Fractal Parameters According to the 3D Roughness-Length Method

Figure 11 shows the log–log plots of the standard deviation, $S(w)$, of residual surface heights, versus the side length, w, of local sampling windows for each square sampling window from the right fracture surface. Nine values of w between 2 and 10 % of the sampling window size were considered. As shown in the figure, all the log-transformed data displayed a linear trend, suggesting that the surfaces are self-affine fractal objects.

Figure 12a, b displays the resulting values of D and A plotted as a function of sampling window size. The values of A display a positive scale effect in agreement with the roughness metrics presented in the preceding subsection. In contrast, the values of D display a negative scale effect. The values of the fractal parameters for each sampling window are provided in Table 6.

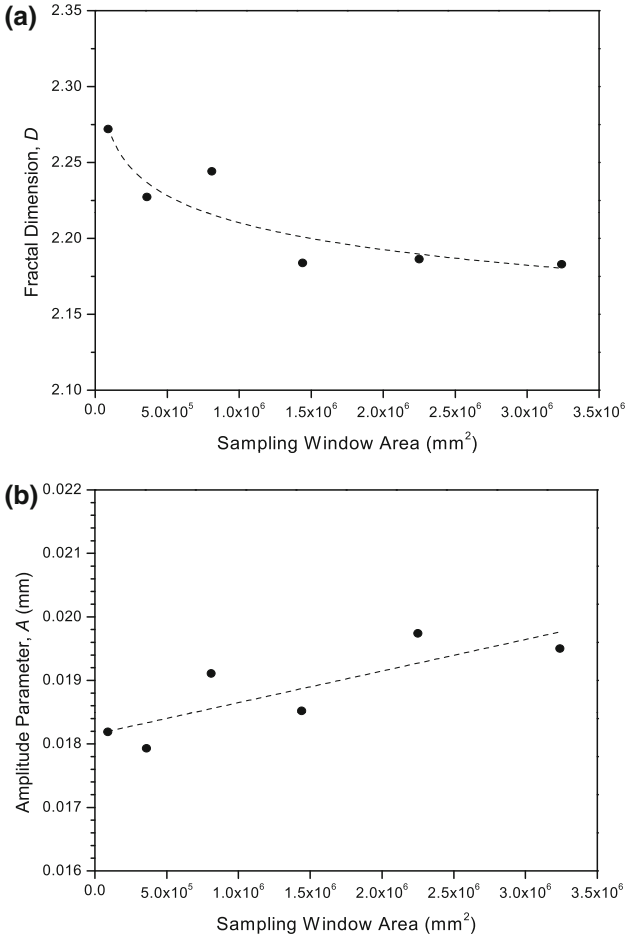

Fig. 12 **a** Fractal dimension (D) and **b** amplitude parameter (A) as a function of sampling window size for the square sampling windows on the right fracture surface

5.4 3D Roughness Coefficient, R_S

The values of the 3D roughness coefficient, R_S, for the sampling windows on the right large-scale fracture surface are plotted in Fig. 13a. A positive scale effect is clearly observed, with the increase in roughness tapering off to a constant value for the larger sampling windows. The values of R_S for each square sampling window are provided in Table 6.

5.5 2D Roughness Coefficients, R_P and Statistical Parameter, Z_2

Figure 14a, b illustrates the polar plots of the 2D roughness coefficient minus one, $R_P - 1$, and the statistical parameter, Z_2, calculated from the 2D profiles extracted from the right fracture surface. $R_P - 1$ was used rather than R_P to generate polar plots, because it allows one to depict the differences in roughness more readily. Since the values of R_P and Z_2 are non-directional, the values in opposing directions (i.e., 0° and 180°) are always equal; thus, the polar plots display inverted symmetry.

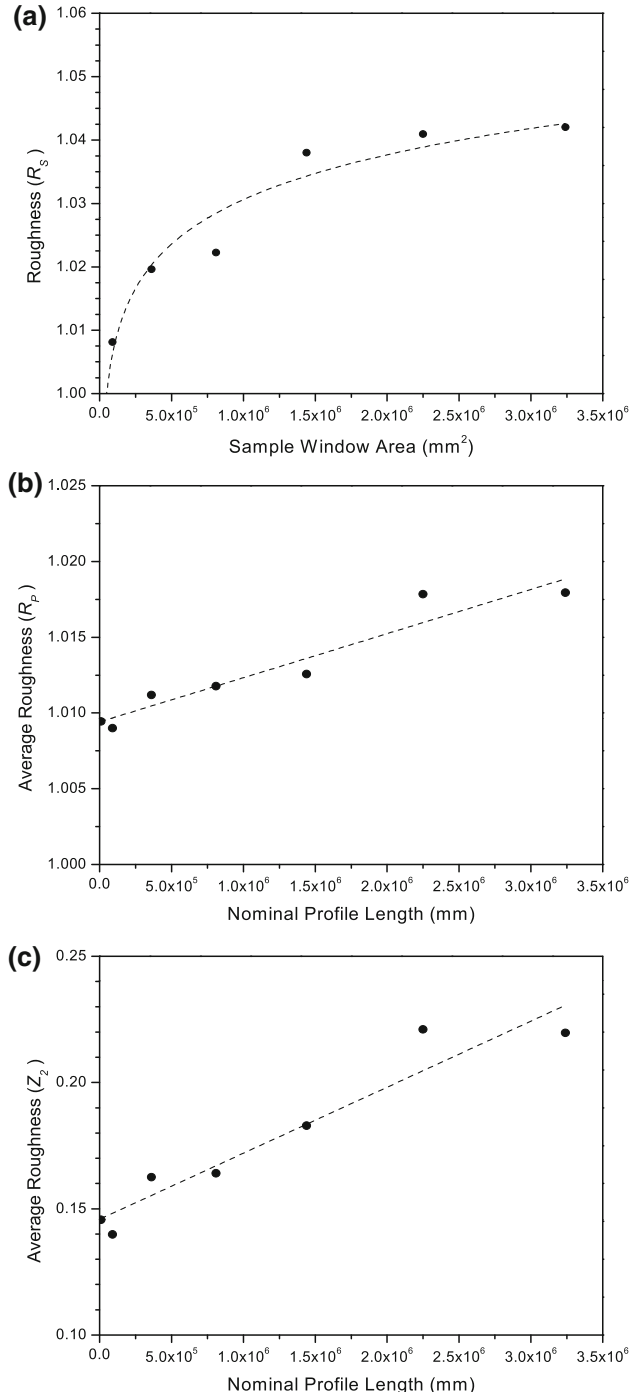

Fig. 13 **a** Values of R_S as a function of sampling window size; **b** average values of R_P as a function of the nominal profile length; and **c** average values of Z_2 as a function of the nominal profile length for the right fracture surface

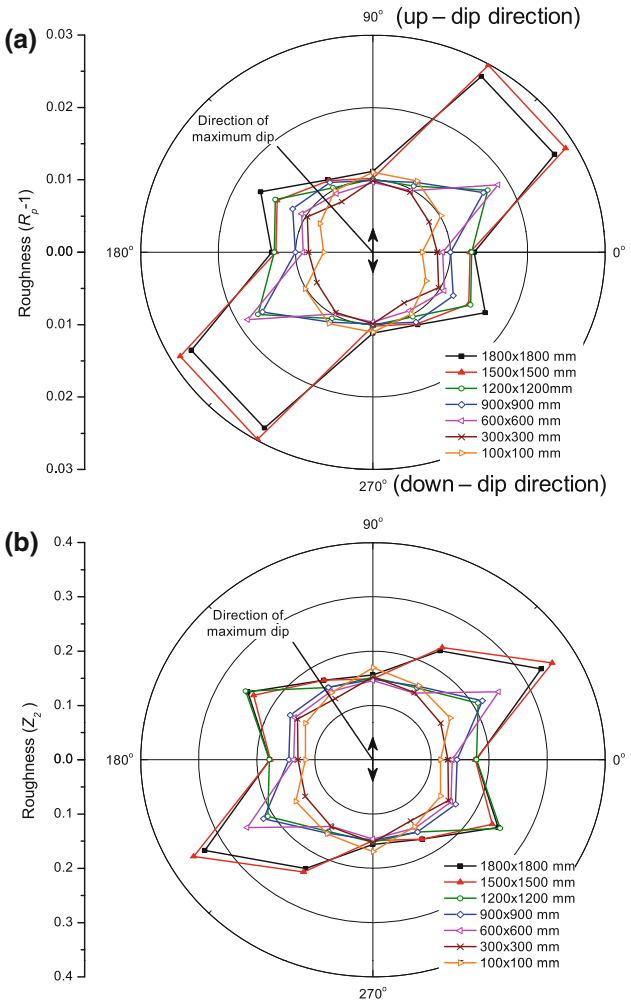

Fig. 14 **a** Polar plots of $R_P - 1$ and **b** Z_2 for the right fracture surface (*note* the 0° and 90° directions are perpendicular and parallel to the up-dip direction defined in Fig. 3b, respectively)

The irregular shape of the data series plotted in Fig. 14 indicates that there is a large variation in the values R_P and Z_2 for 2D profiles extracted from the same surface. Nevertheless, a positive scale effect is observed in many directions (e.g., 150°) in concordance with the majority of alternative roughness values presented herein. The seemingly erratic changes in the values of R_P and Z_2 in the 0°–210°, 60°–240°, and, to a lesser extent, 150°–330° directions were a result of longer profiles encountering large steeply inclined steps on the fracture surface, as previously noted in Fig. 8.[5]

Plots of the average values of R_P and Z_2[6] versus the nominal profile length more clearly illustrate a positive scale effect (Fig. 13b, c), in which the roughness values increase linearly with the profile length considered. The average values of R_P and Z_2 are summarized in Table 6.

6 Influence of Measurement Resolution

6.1 Methodology

To examine the influence of measurement resolution on 3D roughness estimates, the small-scale fracture samples digitized in the laboratory at different resolutions were analyzed. Similar to the investigation of the influence of window size, the best-fit plane through each sample was used as a reference plane for measuring roughness. Also similar to the investigation of window size, the sensitivity of 2D roughness values to resolution was investigated by extracting and analyzing six 2D profiles of equal length oriented at 30° increments from the TIN models of each sample.

6.2 Results of Directional Roughness Evaluation

Figure 15 illustrates the 75 × 75-mm^2 area of Sample 1 digitized with each of the four ATOS configurations listed in Table 3. From this figure, the general influence of measurement resolution on the surface roughness can be observed. That is, surface details are lost as the nominal point spacing increases (i.e., measurement resolution decreases), which effectively smoothes the fracture surface. Hence, surfaces digitized with lower resolution may be characterized by lower roughness parameter values. This relationship was confirmed by the results of 3D and 2D roughness analyses of laboratory-scale samples, as demonstrated in Fig. 16. That is, the roughness estimates decreased with increased nominal point spacing. The results for the three laboratory-scale samples are summarized in Table 7.

The average 3D and 2D roughness values (i.e., the mean of the values at each orientation) for the laboratory-scale samples showed a sizeable difference over the range of nominal point spacing considered (0.044–1 mm) (Fig. 17). Recalling that the measurement noise to nominal point spacing ratio was on the same order of magnitude for each ATOS configuration (Table 4), the increase in the estimated roughness values with resolution can be attributed to the improved digitization accuracy. Considering the average roughness values for all laboratory samples, as given in Table 7, differences of 79–85 and 77–88 % were observed in the 3D and 2D average roughness, respectively. The

[5] In this particular case, 'large' and 'steep' refer to steps in the fracture greater than ~50 mm and inclinations steeper than ~75° measured relative to the best-fit plane through the fracture surface.

[6] The 'average' values of R_P and Z_2 represent the mean of the individual values calculated for each profile.

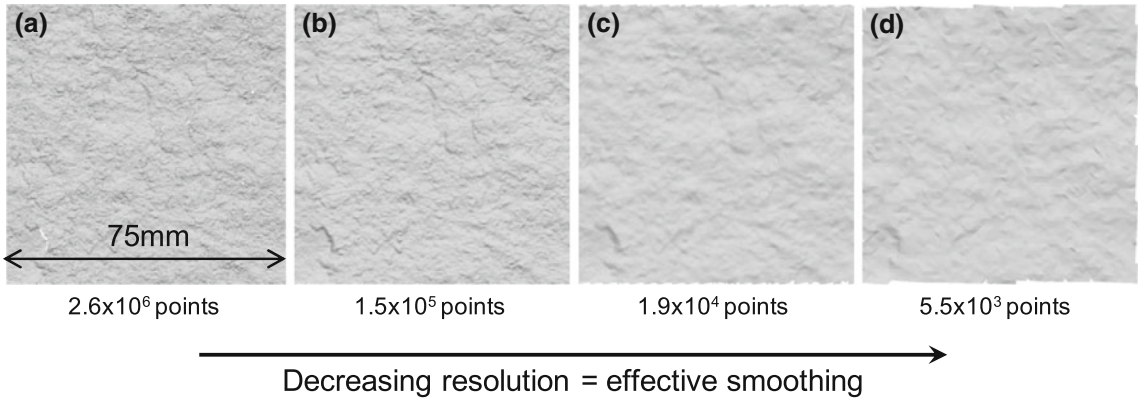

Fig. 15 Example of square sampling area (Sample 1) considered to investigate the influence of measurement resolution. **a**, **b**, **c**, **d** The effective smoothing of 3D surface models resulting from decreased measurement resolution

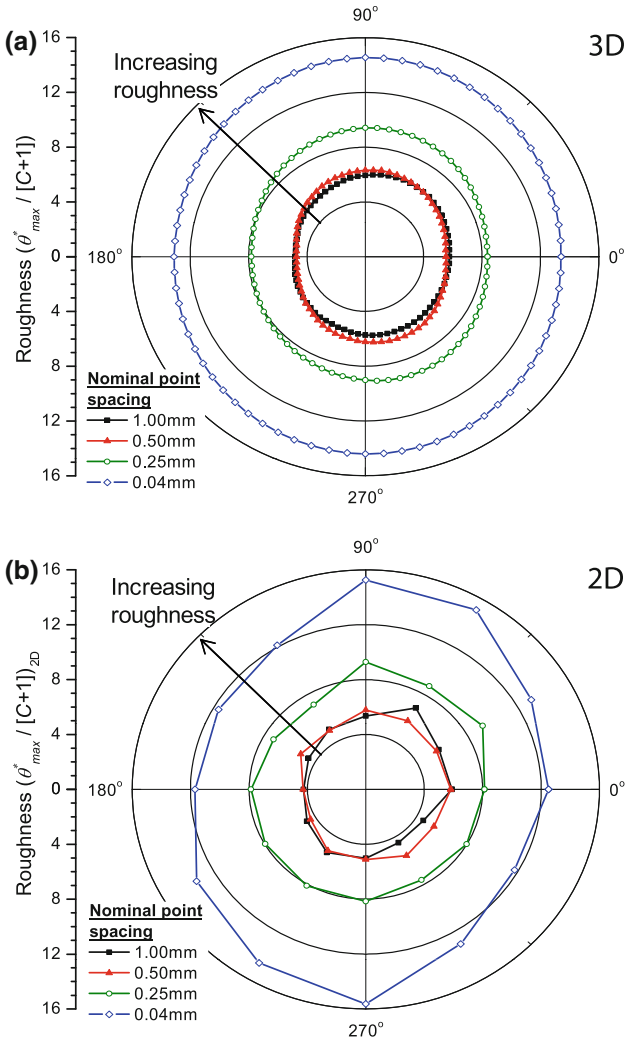

Fig. 16 **a**, **b** Polar plots of the 3D and 2D directional roughness ($\theta^*_{max}/[C+1]$ and $\theta^*_{max}/[C+1]_{2D}$), respectively, for Sample 2 (*note* the orientations of 0°, 90°, 180°, and 270° with respect the specimen are defined in Fig. 4)

average 2D values were consistently lower than the 3D values. From the 2D and 3D values, it is evident that the variation in roughness related to measurement resolution is far greater than that related to sampling window size.

The elliptical shape of the polar plots of the 3D and 2D roughness values indicates that there is roughness anisotropy. These plots indicate that the surface is less rough in the 0°–180° direction versus the 90°–270° direction. The discrepancy in the directional anisotropy between the large-scale surface and small-scale samples is attributed to the orientation of the samples. Although the sampling location and exact line of maximum dip were not recorded for the small-scale fracture samples, the horizontal direction in Fig. 4 roughly defined the line of maximum dip (i.e., perpendicular to the in situ fracture surface). No clear trend in anisotropy as a function of measurement point spacing was observed for the three laboratory-scale samples.

6.3 Results of Non-Directional Roughness Evaluation

6.3.1 Fractal Parameters According to the 3D Roughness-Length Method

Figure 18 illustrates the log–log plots of $S(w)$ versus w for Sample 2. The four log–log plots correspond to each measurement resolution. Local window sizes ranging from 2 to 10 % of the size of the side length of the TIN surface were adopted for the high-resolution ATOS configurations (3 and 4 in Table 3). Slightly larger local window sizes between 3 and 20 % of the side length were adopted when using the lower-resolution ATOS configurations (1 and 2 in Table 3). In doing so, all the log-transformed data displayed a linear trend, which again suggests that the sample surfaces are self-affine fractal objects.

Table 7 Summary of roughness parameters obtained for the three laboratory-scale fracture samples digitized with varying measurement resolution

Nominal point spacing (mm)	Discontinuity roughness						
	Mean $\theta^*_{max}/[C+1]$	Mean $\theta^*_{max}/[C+1]_{2D}$	D	A	R_S	Mean R_P	Mean Z_2
Sample 1							
1.000	5.09	4.65	2.402	0.0188	1.0114	1.0056	0.106
0.500	5.45	5.11	2.253	0.0140	1.0132	1.0065	0.114
0.250	8.25	7.71	2.320	0.0188	1.0308	1.0156	0.179
0.044	12.44	11.47	2.424	0.0247	1.0744	1.0377	0.288
Sample 2							
1.000	5.59	5.11	2.211	0.0138	1.0154	1.0076	0.123
0.500	5.76	5.32	2.174	0.0128	1.0173	1.0084	0.130
0.250	8.68	8.16	2.332	0.0204	1.0372	1.0186	0.198
0.044	13.87	13.20	2.448	0.0286	1.0934	1.0525	0.359
Sample 3							
1.000	5.88	5.52	2.322	0.0179	1.0191	1.0074	0.122
0.500	5.90	5.69	2.184	0.0130	1.0206	1.0083	0.129
0.250	8.81	8.52	2.325	0.0198	1.0397	1.0189	0.199
0.044	13.26	12.49	2.415	0.0256	1.0832	1.0451	0.327

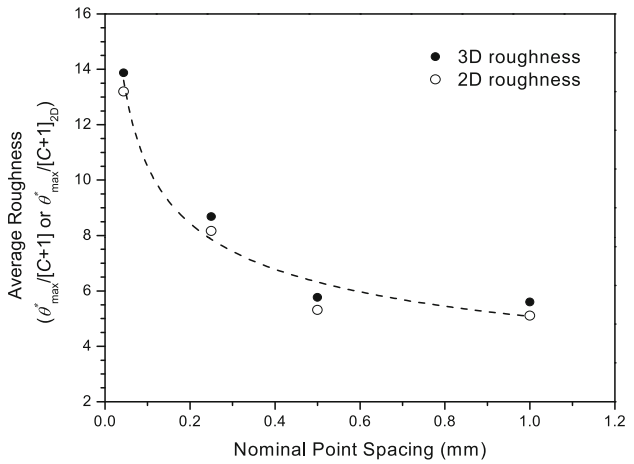

Fig. 17 Average 3D and 2D directional roughness (mean $\theta^*_{max}/[C+1]$ and mean $\theta^*_{max}/[C+1]_{2D}$) as a function of the nominal point spacing (measurement resolution) used to digitize Sample 2

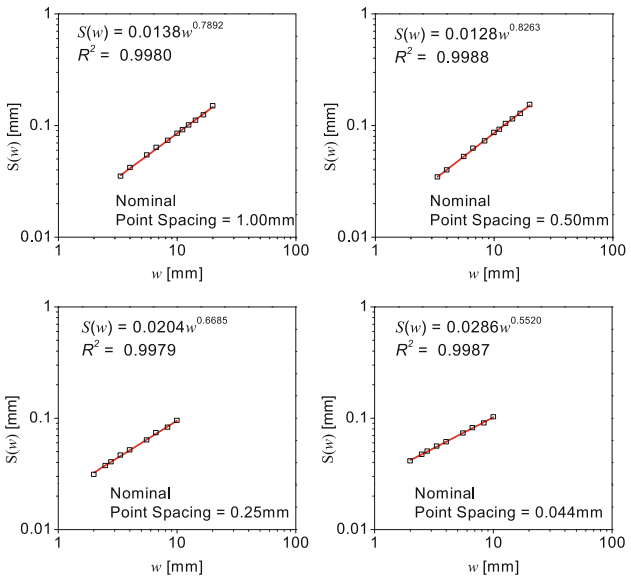

Fig. 18 Log–log plots of $S(w)$ versus w for Sample 2 when digitized with nominal point spacings of 1.0, 0.50, 0.25, and 0.044 mm

The plots of D and A as function of the nominal point spacing for Sample 2 are shown in Fig. 19. These parameters decrease with decreasing resolution similar to the other measures of roughness. A summary of the values for each sample is included in Table 7.

6.4 3D Roughness Coefficient, R_S

The values of the 3D roughness coefficient, R_S, for Sample 2 are plotted in Fig. 20a. A clear decrease in roughness with increasing nominal point spacing is shown. The values of R_S for each laboratory sample are provided in Table 7.

6.5 2D Roughness Coefficient, R_P and Statistical Parameter, Z_2

Figure 21 illustrates the polar plots of the 2D roughness coefficient minus one, $R_P - 1$, and the statistical

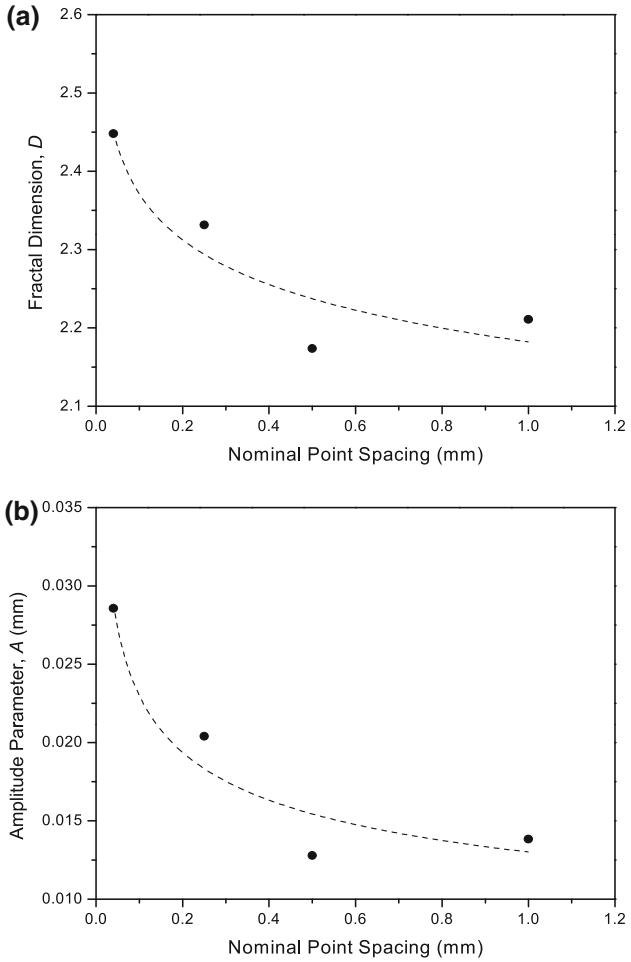

Fig. 19 **a** Fractal dimension (D) and **b** amplitude parameter (A) as a function of the nominal point spacing (measurement resolution) used to digitize Sample 2

parameter, Z_2, for the six 2D profiles extracted from Sample 2. As before, the polar plots display inverted symmetry because values of R_P and Z_2 are equal in opposing directions (i.e., 0° and 180°). Since the profiles obtained from the fracture samples were much shorter than those taken from the field-scale fracture, they did not contain steps like those that led to erratic variations in R_P and Z_2 presented in Sect. 5. The polar plots demonstrate that both $R_P - 1$ and Z_2 decrease as the nominal measurement point spacing increases in agreement with the other roughness parameters considered herein.

The elliptical shape of the plots is also in agreement with the shape of the polar plots of $\theta^*_{max}/[C+1]$ and $\theta^*_{max}/[C+1]_{2D}$ with the maximum and minimum roughness encountered in the 90°–270° and 0°–180° directions, respectively.

Plots of the average values of R_P and Z_2 as a function of nominal point spacing also illustrate that roughness

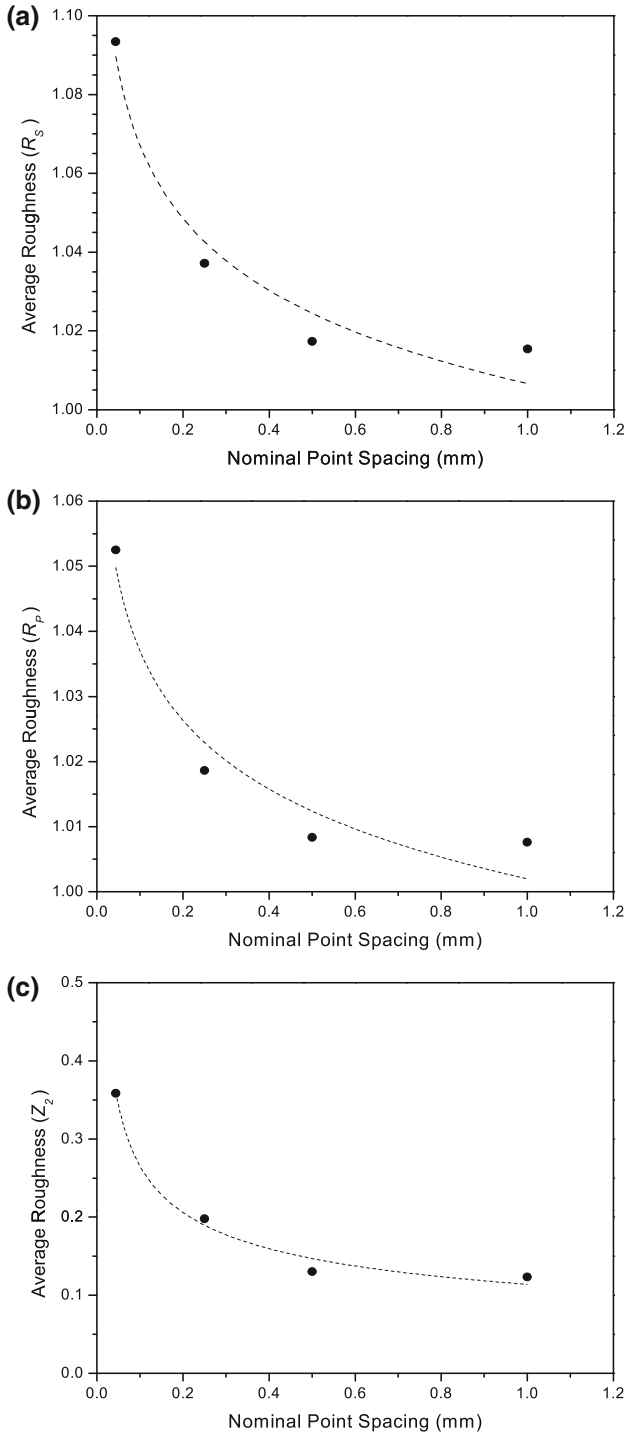

Fig. 20 Values of **a** R_S, **b** mean R_P, and **c** mean Z_2 as a function of the nominal point spacing (measurement resolution) used to digitize Sample 2

decreases with increasing nominal point spacing (Fig. 20b, c). The values of R_P and Z_2 for each laboratory sample are provided in Table 7. Comparison of R_P, to R_s shows that the 2D values are consistently lower than their 3D counterparts.

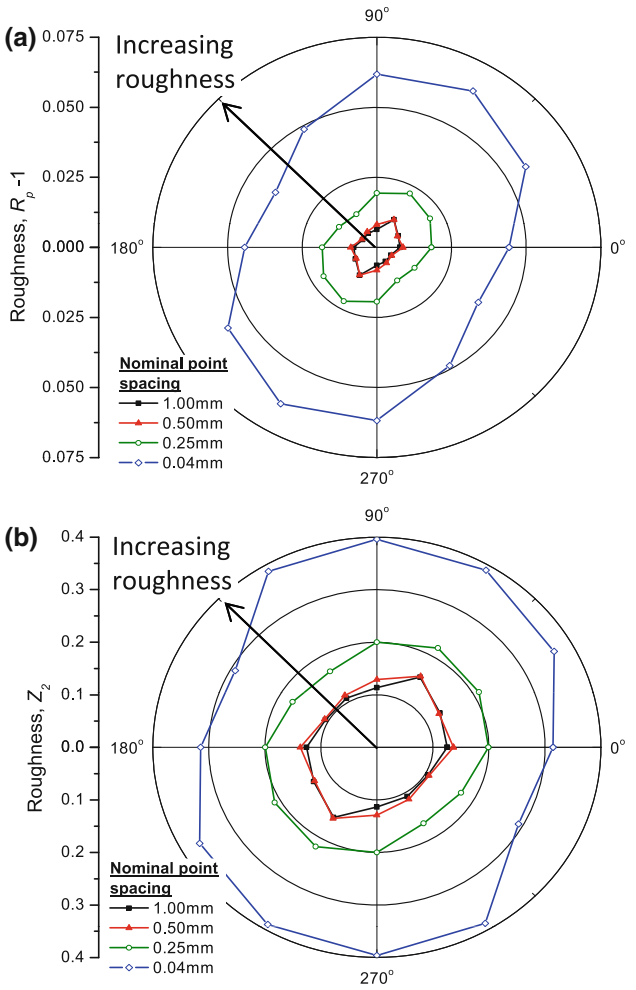

Fig. 21 **a** Polar plots of $R_P - 1$ and **b** Z_2 for Sample 2 (*note* the orientations of 0°, 90°, 180°, and 270° with respect the specimen are defined in Fig. 4)

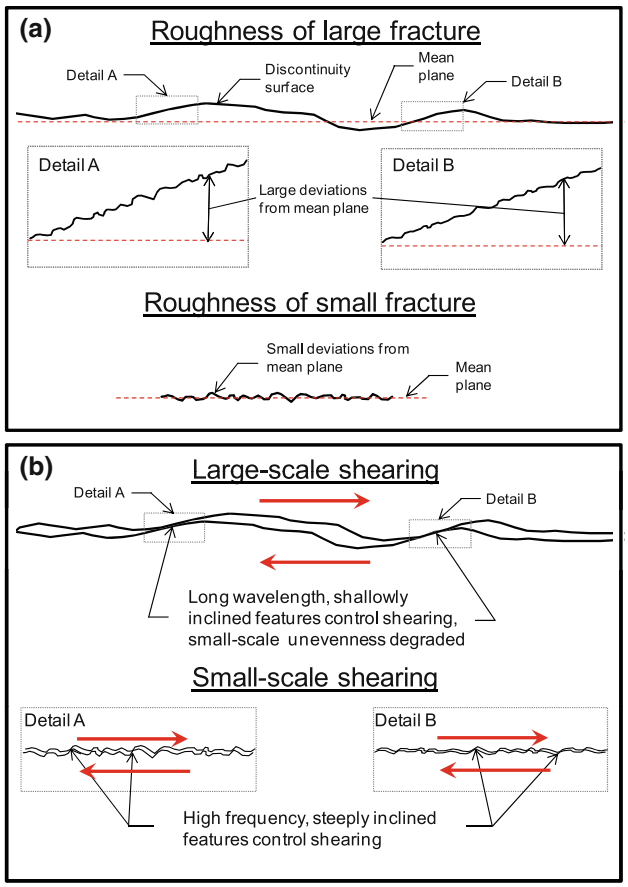

Fig. 22 **a** Schematic of roughness (waviness + unevenness) for a large and small fracture and **b** schematic showing asperities involved in the shearing process for large and small asperities

7 Discussion

7.1 Window Size

Prior to the current study, several other researchers investigated the scale dependence of rock discontinuity roughness and shear strength (see Table 1) with mixed results. With the exception of the fractal dimension, D, the results from the current study displayed a positive scale effect. Recalling that all sampling windows were digitized with a constant nominal point spacing of 1 mm, larger sampling windows included larger-scale waviness along with the small-scale unevenness component of roughness. As a result of the combination of these components, larger values of the various roughness parameters were obtained. Moreover, increasingly larger windows contained more steps in the fracture surface that significantly increased the value of some roughness parameters. Since such steps on a discontinuity surface often exert control on the shear resistance, it is considered beneficial for roughness parameters to be sensitive to the presence of such features.

A positive roughness scale effect suggests that the decrease in shear resistance associated with increased discontinuity size may not necessarily be a result of a decrease in roughness as typically assumed. When considering this seemingly controversial positive scale effect, it is important to recall that Barton and co-workers (Barton 1976; Barton and Choubey 1977; Barton and Bandis 1982, 1990) and Bandis et al. (1981) postulated that it is the effective asperity size that changes with increasing scale. That is not to say that the roughness, defined by Brady and Brown (2005) as the inherent surface waviness and unevenness of a discontinuity relative to its mean plane, decreases with scale.

For larger discontinuities, the larger-scale roughness components seem to control the shear behavior as the smaller-scale roughness components suffer immediate degradation with shear displacement. As larger-scale roughness components tend to be of a longer wavelength, they appear smoother compared to the small-scale roughness components. Thus, it appears that the 'effective' roughness decreases. An important distinction must be made between

roughness (unevenness + waviness) and 'effective' roughness. Figure 22 contains two schematics to aid in distinguishing between these terms. Confusion between these terms may partly explain the conflicting view on roughness scale effects presented in previous studies.

With the shear resistance of large-scale discontinuities apparently controlled by larger-scale roughness, one may argue that the large-scale and small-scale roughness must be characterized separately. However, defining the division between these scales in a methodical manner is complicated by the lack of a definitive wavelength cutoff. By measuring surface topography with point spacing $\leq$1 mm over area of several square metres, which is now a practical task, both scales of roughness can be captured simultaneously eliminating the need to separate the data collection procedures. The way in which this total roughness influences the shear strength at different scales and translates into different 'effective' roughness requires further study of the kinematics of the shearing process. Using high-resolution surface measurements, like those acquired in the current study, it is envisaged that a better understanding of this process can be gained via simulation of large-scale direct shear tests using advanced numerical methods (e.g., Karami and Stead 2008; Tatone and Grasselli 2012a).

Also of note is that the 3D roughness values presented herein approached a constant value as larger sampling windows were considered. Diminishing scale effects with increasing scale had been suggested by Barton and Bandis (1982) and has been shown by Lanaro et al. (1999), Lanaro (2000) and Fardin et al. (2001). The latter two authors refer to the area at which roughness estimates become constant as a roughness stationarity limit and suggest that roughness be estimated from surface measurements that extend over areas at least equal to this limit.

7.2 Measurement Resolution

Discontinuity roughness can be considered a continuous signal with an unknown frequency range. Every device available to measure discontinuity surface topography acts as an implicit bandpass filter, in that some high- and low-frequency components (i.e., small- and large-scale roughness components) of the surface topography cannot be captured. High-frequency filtering is caused by a combination of sampling limitations, namely the minimum possible point spacing (i.e., horizontal distance between subsequent measurement points) and the size of the sampling aperture (i.e., the diameter of a stylus or laser beam on the discontinuity surface) (Poropat 2009), while low-frequency filtering is a result of the limited discontinuity surface area available for measurement.

Digitization of a surface with reduced resolution results in the distortion and loss of the original characteristics of the surface, a process known as 'aliasing' (e.g., Fig. 15). Several previous studies of laboratory-scale 2D profiles have shown that the measurement resolution influences statistical and fractal roughness parameters (Huang et al. 1992; Kulatilake et al. 1995; Seidel and Haberfield 1995, amongst others), in particular aliasing results in the underestimation of roughness parameters (e.g., Yu and Vayssade 1991; Hong et al. 2008). The outcomes of the current study are in agreement, as they show that decreasing measurement resolution can significantly reduce estimates of 2D and 3D surface roughness parameters.

In this study, roughness parameters were shown to decrease by up to 88 % as the nominal measurement point spacing was increased from 0.044 to 1 mm. This sensitivity to measurement resolution is far more significant compared to the sensitivity in roughness related to sample size. Consequently when measuring the roughness of any discontinuity of any size, it is very important to clearly express the measurement resolution that has been employed to digitize the surface and to ensure it remains constant for all measurements. Failure to do so will render the resulting roughness parameters incomparable. The use of consistent measurement resolution has particular significance when using any empirical shear strength criterion that incorporates roughness parameters. These strength criteria were established using roughness parameters derived from surface measurements acquired at some specific resolution. Failure to the same resolution could lead to significant errors in discontinuity shear strength estimates.

Some of the conflicting positive and negative scale effects observed in previous studies that involved measuring large-scale surfaces (i.e., profiles or surfaces $\geq$1 m or 1 m^2, respectively) may be attributed to confusion between the influence of sample size and influence of measurement resolution. Of all the studies on large-scale fractures in the literature (i.e., Maerz and Franklin 1990; Cravero et al. 2001; Fardin et al. 2001, 2004; Feng et al. 2003), all but Fardin et al. (2004) utilized inconsistent measurement resolutions when digitizing surfaces of varying size. In these studies, the nominal measurement point spacing was increased as larger areas (or lengths) of the fracture surface were characterized leading to a higher degree of aliasing. Hence, it is possible that the decrease in roughness with increased discontinuity size observed in those studies was a consequence of the changing measurement resolution and not a change in roughness (unevenness + waviness).

Fardin et al. (2004) maintained a consistent measurement resolution and found that the 3D fractal parameters, D and A, decreased with increasing window size to consistent minimum values for windows larger than 3,000 $\times$ 3,000 mm^2. The values of D for the field-scale discontinuity in the current study also showed a negative

scale effect, which approached a constant value for larger sampling windows. However, the values of A obtained in the current study showed a positive scale effect. This discrepancy between the study of Fardin et al. (2004) and the current study may be partly attributed to the measurement resolution. The nominal point spacing used by Fardin et al. (2004) was an order of magnitude larger compared to that used in the current study (20 vs. 1 mm). Thus, smaller-scale features of the surface were neglected from roughness evaluations. This hypothesis is supported by the results of a more recent study of four fracture replicas of varying size by Fardin (2008). In this later study, higher resolution measurements (0.2-mm nominal point spacing) were used and both D and A displayed a positive scale effect.

The question remains as to what resolution is ideal to characterize roughness. At present, there are no widely adopted methods or suggested guidelines to determine what resolution (nominal point spacing) should be used to measure discontinuity roughness. Reeves (1985) stated that the selected measurement sampling interval and aperture (resolution) should capture all those "frequencies relevant to the problem to which the data are applied". For discontinuity shear strength, the frequencies of interest would appear to be those that encompass the asperities involved in the shearing process. Recent work by the authors on selected laboratory-scale fracture replicas has shown that the measurement point spacing must be less than 0.5 mm to capture the relevant asperities (Tatone et al. 2010). In considering larger-scale discontinuities, further work is required to determine the resolution needed to capture the asperities governing the shearing process (i.e., effective roughness). Until our understanding improves, the highest practical resolution should always be used for discontinuity surface measurements.

7.3 Influence of Selected Reference Plane

Swan and Zongqi (1985) showed that both positive and negative roughness scale effects could be observed from a single 2D profile by changing the line of reference used to calculate the roughness. When considering several subsamples of a longer profile:

- a positive scale effect was observed when a unique best-fit reference line for each sample was used to measure the roughness and
- a negative scale effect was observed when a common best-fit line through the entire profile was used to measure the roughness.

For the current study, a unique best-fit plane was established for each sampling window and a positive scale effect was observed. Hence, the same fracture surface, analyzed using a common best-fit plane as the reference plane, could potentially display a negative scale effect. To quickly examine the effect of the selected reference plane, the 3D roughness, $\theta^*_{max}/[C+1]$ was recalculated using a common reference plane for all sampling windows (the best-fit plane of the largest window). The resulting polar plots of the right fracture surface are shown in Fig. 23. A positive scale effect is still observed in most analysis directions, although the trend becomes less definitive is some directions (e.g., at 270°). Nonetheless, the average roughness continues to display a well-defined positive scale effect. Such results reinforce the importance of analyzing the roughness of 3D surfaces or many 2D profiles rather than single 2D profiles. Where a single profile may show a positive or negative scale effect depending on the selected line of reference, consideration of the entire surface will continue to display a positive scale effect.

7.4 Relationship Between Roughness Scale Effects and Shear Strength Scale Effects

Some further clarification must be made between roughness and shear strength scale effects. The majority of the roughness values presented herein show that discontinuity roughness increases as the size of the discontinuity increases in contrast to the typical downscaling that is applied to the JRC in the Barton–Bandis shear criterion. Such results could potentially lead one to conclude that shear strength should also increase with discontinuity size. However, numerous shear tests on rock joints of varying

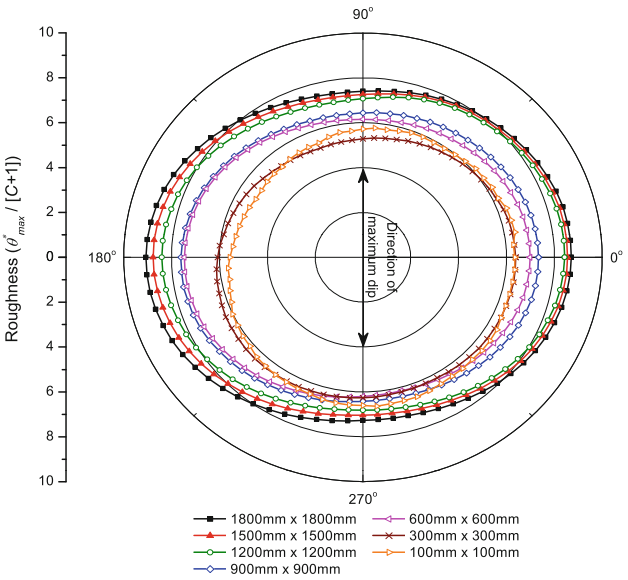

Fig. 23 Polar plots of the 3D directional roughness values ($\theta^*_{max}/[C+1]$) for the square sampling windows of the right fracture surface calculated using the best-fit plane through the largest sampling window as a common reference plane

size reported in the literature indicate that shear strength decreases with sample size (Barton and Bandis 1982).

When using the Barton–Bandis shear strength criterion, it is important to recall that the JRC parameter originated as a curve-fitting parameter and not a direct measure of the waviness and unevenness of a discontinuity surface relative to its mean plane. Hence, the JRC may be more aptly considered a measure of the 'effective' roughness and the downscaling of the JRC value is a reasonable approach to account for the decrease in 'effective' roughness for discontinuities within a narrow size range (0.1–5 m). However, further work is required to fully understand the mechanisms responsible for the decrease in shear strength observed with increasing scale.

8 Summary and Conclusions

Based on the observations and analyses presented in this paper, the major conclusions regarding the measurement of discontinuity roughness and roughness scale effects are as follows:

- The ATOS system adopted in this study was successfully used in situ and in the laboratory to digitize a discontinuity surface. Over the range of measurement resolutions defined by a nominal point spacing of 0.044–1.0 mm, the ATOS system was able to capture data with relatively little noise, which made the measurement data ideal for measuring roughness.
- Evaluating the roughness of sample windows of varying size taken from the out-crop scale discontinuity surface revealed that, in contrast to the conventional view, the estimates of roughness increased as larger areas of the discontinuity surface were considered. The average 3D roughness ($\theta^*_{max}/[C+1]$) over the range of window sizes considered (100×100 mm^2 to $1{,}800 \times 1{,}800$ mm^2) displayed a sizable 34 % difference in roughness. This increase appeared to level off as sampling windows exceeded 3×10^6 mm^2 in size.
- More importantly, it was shown that measurement resolution has a stronger influence on the resulting values compared to the sample window size. The average 3D roughness ($\theta^*_{max}/[C+1]$) was shown to vary by up to 88 % over the range of measurement resolutions considered (i.e., nominal point spacing of 0.44–1.0 mm). Upon reviewing some of the previous studies of the roughness of out-crop scale discontinuity surfaces, it was discovered that the measurement resolution was varied as sample windows of different sizes were considered in nearly all cases. Therefore, it was suggested that the often cited decrease in roughness with increasing sample size may be attributed to inconsistent measurement resolution.

Acknowledgments This work has been supported by the Natural Science and Engineering Research Council of Canada in the form of Discovery Grant No. 341275 and RTI Grant No. 345516 held by G. Grasselli and a Canada Graduate Scholarship held by B.S.A. Tatone. The authors would also like to thank Pulin Mondal for his assistance with the field work required for this study.

References

Baker BR, Gessner K, Holden E-J, Squelch AP (2008) Automatic detection of anisotropic features on rock surfaces. Geosph 4(2): 418–428

Bandis S, Lumsden AC, Barton NR (1981) Experimental studies of scale effects on the shear behavior of rock joints. Int J Rock Mech Min Sci Geomech Abstr 18(1):1–21

Barton N (1973) Review of a new shear-strength criterion for rock joints. Eng Geol 7(4):287–332

Barton N (1976) Shear-strength of rock and rock joints. Int J Rock Mech Min Sci Geomech Abstr 13(9):255–279

Barton N, Bandis S (1982) Effects of block size on the shear behaviour of jointed rock. In: Proceedings of the 23rd US rock mechanics symposium, Berkeley, CA, August 1982, pp 739–760

Barton N, Bandis S (1990) Review of predictive capabilities of JRC-JCS model in engineering practice. In: Barton N, Stephansson O (eds) Rock joints: proceedings of the international symposium on rock joints, Loen, Norway, 4–6 June 1990. A. A. Balkema, Rotterdam, pp 603–610

Barton N, Choubey V (1977) The shear strength of rock joints in theory and practice. Rock Mech Rock Eng 10(1):1–54

Belem T, Homand-Etienne F, Souley M (1997) Fractal analysis of shear joint roughness. Int J Rock Mech Min Sci 34(3–4): paper 130

Brady BHG, Brown ET (2005) Rock mechanics for underground mining, 3rd edn. Kluwer Academic Publishers, New York

Brown SR (1995) Simple mathematical model of a rough fracture. J Geophys Res 100((B4)):5941–5952

Brown SR, Scholz CH (1985) Broad bandwidth study of the topography of natural rock surfaces. J Geophys Res 90((B14)): 2575–2582

Castelli M, Re F, Scavia C, Zaninetti A (2001) Experimental evaluation of scale effects on the mechanical behavior of rock joints. In: Sarkka P, Eloranta P (eds) Rock mechanics—a challenge for society; proceedings of Eurock 2001, Espoo, Finland, 4–7 June 2001. A.A. Balkema, Rotterdam, pp 205–210

Chae BG, Ichikawa Y, Jeong GC, Seo YS, Kim BC (2004) Roughness measurement of rock discontinuities using a confocal laser scanning microscope and the Fourier spectral analysis. Eng Geol 72(3–4):181–199

Cravero M, Iabichino G, Piovano V (1995) Analysis of large joint profiles related to rock slope instabilities. In: 8th ISRM congress, Tokyo, Japan, 25–29 September 1995. A.A. Balkema, Rotterdam, pp 423–428

Cravero M, Iabichino G, Ferrero AM (2001) Evaluation of joint roughness and dilatancy of schistosity joints. In: Sarkka P, Eloranta P (eds) Rock mechanics—a challenge for society; proceedings of Eurock 2001, Espoo, Finland, 4–7 June 2001. A.A. Balkema, Rotterdam, pp 217–222

El-Soudani SM (1978) Profilometric analysis of fractures. Metallography 11(3):247–336

Fardin N (2008) Influence of structural non-stationarity of surface roughness on morphological characterization and mechanical deformation of rock joints. Rock Mech Rock Eng 41(2):267–297

Fardin N, Stephansson O, Jing L (2001) The scale dependence of rock joint surface roughness. Int J Rock Mech Min Sci 38(5):659–669

Fardin N, Feng Q, Stephansson O (2004) Application of a new in situ 3D laser scanner to study the scale effect on the rock joint surface roughness. Int J Rock Mech Min Sci 41(2):329–335

Fecker E, Rengers N (1971) Measurement of large scale roughness of rock planes by means of profilograph and geological compass. In: Proceedings of the 1st ISRM symposium, Nancy, France, 1971, pp 1–18

Feng Q, Fardin N, Jing L, Stephansson O (2003) A new method for in situ non-contact roughness measurement of large rock fracture surfaces. Rock Mech Rock Eng 36(1):3–25

Giani GP, Ferrero AM, Passarello G, Reinaudo L (1995) Scale effect evaluation on natural discontinuity shear strength. In: Myers LR, Tsang CF, Cook NGW, Goodman RE (eds) Proceedings of the conference on fractured and jointed rock masses, Lake Tahoe, CA, 3–5 June 1992. A.A. Balkema, Rotterdam, pp 447–452

GOM (2008) ATOS user manual v. 6.1. GOM mbH, Braunschweig, Germany

Grasselli G (2006) Manuel Rocha medal recipient—shear strength of rock joints based on quantified surface description. Rock Mech Rock Eng 39(4):295–314

Grasselli G, Wirth J, Egger P (2002) Quantitative three-dimensional description of a rough surface and parameter evolution with shearing. Int J Rock Mech Min Sci 39(6):789–800

Haneberg W (2007) Directional roughness profiles from three-dimensional photogrammetric or laser scanner point clouds. In: Eberhardt E, Stead D, Morrison T (eds) Rock mechanics: meeting society's challenges and demands; proceedings of the 1st Canada–US rock mechanics symposium, Vancouver, Canada, 27–31 May 2007. Taylor and Francis, London, pp 101–106

Hencher SR, Toy JP, Lumsden AC (1993) Scale-dependent shear-strength of rock joints. In: Pinto Da Cunha A (ed) Scale effects in rock masses 93; proceedings of the 2nd international workshop on scale effects in rock masses, Lisbon, Portugal, 25 June 1993. A.A. Balkema, Rotterdam, pp 233–240

Hong ES, Lee IM, Lee JS (2006) Measurement of rock joint roughness by 3D scanner. Geotech Test J 29(6):482–489

Hong ES, Lee JS, Lee IM (2008) Underestimation of roughness in rough rock joints. Int J Numer Anal Meth Geomech 32(11): 1385–1403

Huang SL, Oelfke SM, Speck RC (1992) Applicability of fractal characterization and modelling to rock joint profiles. Int J Rock Mech Min Sci Geomech Abstr 29(2):89–98

ISRM (1978) International Society for Rock Mechanics commission on standardization of laboratory and field tests: suggested methods for the quantitative description of discontinuities in rock masses. Int J Rock Mech Min Sci Geomech Abstr 15(6): 319–368

Karami A, Stead D (2008) Asperity degradation and damage in the direct shear test: a hybrid FEM/DEM approach. Rock Mech Rock Eng 41(2):229–266

Kulatilake PHSW, Um J (1999) Requirements for accurate quantification of self-affine roughness using the roughness-length method. Int J Rock Mech Min Sci 36(1):5–18

Kulatilake PHSW, Shou G, Huang TH, Morgan RM (1995) New peak shear strength criteria for anisotropic rock joints. Int J Rock Mech Min Sci Geomech Abstr 32(7):673–697

Kulatilake P, Balasingam P, Park J, Morgan R (2006) Natural rock joint roughness quantification through fractal techniques. Geotech Geol Eng 24(5):1181–1202

Kutter HK, Otto F (1990) Influence of parallel and cross-joints on shear behaviour of rock discontinuities. In: Barton N, Stephansson O (eds) Rock joints, Loen, Norway, 4–6 June 1990. A.A. Balkema, Rotterdam, pp 243–250

Lanaro F (2000) A random field model for surface roughness and aperture of rock fractures. Int J Rock Mech Min Sci 37(8): 1195–1210

Lanaro F, Jing L, Stephansson O (1999) Scale dependency of roughness and stationarity of rock joints. In: Vouille G, Berest P (eds) Proceedings of the 9th congress of ISRM, Paris, France, 25–28 August 1999, pp 1391–1395

Lee H-S, Ahn K-W (2004) A prototype of digital photogrammetric algorithm for estimating roughness of rock surface. Geosci J 8(3):333–341

Leal-Gomes MJA (2003) Some new essential questions about scale effects on the mechanics of rock joints. In: Handley M (ed) Proceedings of the 10th ISRM Congress: Technology roadmap for rock mechanics. Sandton, South Africa, South African Institute of Mining and Metallurgy, pp 721–727

Maerz NH, Franklin JA (1990) Roughness scale effects and fractal dimension. In: Pinto Da Cunha A (ed) Scale effects in rock masses; proceedings of the first international workshop on scale effects in rock masses, Loen, Norway, 7–8 June 1990. A.A. Balkema, Rotterdam, pp 121–125

Malinverno A (1990) A simple method to estimate the fractal dimension of a self-affine series. Geophys Res Lett 17(11): 1953–1956

Mandelbrot B (1967) How long is the coast of Britain? Statistical self-similarity and fractional dimension. Science 156(3775):636–638

Mandelbrot B (1983) The fractal geometry of nature. W.H. Freeman, New York

McWilliams PC, Kerkering JC, Miller SM (1990) Fractal characterization of rock fracture roughness for estimating shear strength. In: Rossmanith HP (ed) Mechanics of jointed and faulted rock, Vienna, 18–20 April 1990. A.A. Balkema, Rotterdam, pp 331–336

Muralha J, Pinto Da Cunha A (1990) About LNEC experience on scale effects in the mechanical behaviour of rocks. In: Pinto Da Cunha A (ed) Scale effects in rock masses; proceedings of the first international workshop on scale effects in rock masses, Loen, Norway, 7–8 June 1990. A.A. Balkema, Rotterdam, pp 131–148

Myers NO (1962) Characterization of surface roughness. Wear 5(3):182–189

Nasseri MHB, Tatone BSA, Grasselli G, Young RP (2009) Fracture toughness and fracture roughness interrelationship in thermally treated Westerly granite. Pure Appl Geophys 166(5): 801–822

Ohnishi Y, Yoshinaka R (1995) Laboratory investigation of scale effect in mechanical behaviour of rock. In: Myers LR, Tsang CF, Cook NGW, Goodman RE (eds) Proceedings of the conference on fractured and jointed rock masses, Lake Tahoe, CA, 3–5 June 1992. A.A. Balkema, Rotterdam, pp 465–477

Poropat GV (2009) Measurement of surface roughness of rock discontinuities. In: Grasselli G, Diederichs MS (eds) Rock engineering in difficult conditions; proceedings of 3rd Canada-US rock mechanics symposium, Toronto, Canada, 9–15 May 2009, Paper 3976

Pratt HR, Black AD, Brace WF (1974) Friction and deformation of jointed quartz diorite. In: Advances in rock mechanics; reports of current research; proceedings of the 3rd congress of ISRM, Denver, CO, 1–7 September 1974. National Academy of Sciences, Washington, DC, pp 306–310

Rahman Z, Slob S, Hack R (2006) Deriving roughness characteristics of rock mass discontinuities from terrestrial laser scan data. In: Proceedings of IAEG2006: engineering geology for tomorrow's cities, Nottingham, UK, 6–10 September 2006. The Geological Society of London, London, UK, Paper 437

Rasouli V, Harrison JP (2004) A comparison of linear profiling and an in-plane method for the analysis of rock surface geometry. Int J Rock Mech Min Sci 41(3):377–378

Reeves MJ (1985) Rock surface roughness and frictional strength. Int J Rock Mech Min Sci Geomech Abstr 22(6):429–442

Riss J, Gentier S (1990) Angularity of a natural rock fracture. In: Rossmanith HP (ed) Mechanics of jointed and faulted rock, Vienna, 18–20 April 1990. A.A. Balkema, Rotterdam, pp 399–406

Seidel JP, Haberfield CM (1995) Towards an understanding of joint roughness. Rock Mech Rock Eng 28(2):69–92

Swan G, Zongqi S (1985) Prediction of shear behaviour of joints using profiles. Rock Mech Rock Eng 18(3):183–212

Tatone BSA, Grasselli G (2009) A method to evaluate the three-dimensional roughness of fracture surfaces in brittle geomaterials. Rev Sci Instrum 80(12), Paper 125110

Tatone BSA, Grasselli G (2010) A new 2D discontinuity roughness parameter and its correlation with JRC. Int J Rock Mech Min Sci 47(8):1391–1400

Tatone BSA, Grasselli G (2012a) Modeling direct shear tests with FEM/DEM: Investigation of discontinuity shear strength scale effect as an emergent characteristic In: 46th US rock mechanics symposium, Chicago, Paper 651

Tatone BSA, Grasselli G (2012b) Quantitative measurements of fracture aperture and directional roughness from rock cores. Rock Mech Rock Eng 45(4):619–629

Tatone BSA, Grasselli G, Cottrell B (2010) Accounting for the influence of measurement resolution on discontinuity roughness estimates. In: Eurock; rock mechanics in civil and environmental engineering, Lausanne, Switzerland, 15–18 June 2010. A.A. Balkema, Rotterdam, pp 203–206

Turk N, Grieg MJ, Dearman WR, Amin FF (1987) Characterization of rock joint surfaces by fractal dimension. In: Farmer IW, Daeman JJK, Desai CS, Glass CE, Neuman SP (eds) Proceedings of 28th US rock mechanics symposium, Tuscon, AZ, 29 June–1 July 1987. A.A. Balkema, Rotterdam, pp 1223–1236

Yu XB, Vayssade B (1991) Joint profiles and their roughness parameters. Int J Rock Mech Min Sci Geomech Abstr 28(4): 333–336